

Higher-Point Correlators in $\mathcal{N} = 4$ SYM: Ten-Dimensional Null Polygons

TILL BARGHEER¹, ALBERT BEKOV¹, CARLOS BERCIÑI¹, FRANK CORONADO²

¹ *Deutsches Elektronen-Synchrotron DESY, Notkestr. 85, 22607 Hamburg, Germany*

² *Institut für Theoretische Physik, ETH Zurich, CH-8093 Zürich, Switzerland*

till.bargheer@desy.de, albert.bekov@desy.de,
carlos.bercini@desy.de, fcidrogo@gmail.com

Abstract

We consider higher-point generalizations of the “octagon” large-charge four-point function in planar $\mathcal{N} = 4$ super Yang–Mills theory. These n -point polygon correlators are defined as ten-dimensional null limits of generating functions of n -point correlators of protected scalar operators with arbitrary R-charge, and are conjecturally dual to massive scattering amplitudes of W-bosons on the Coulomb branch of the theory. We present a twistor-based direct computation of the polygon loop integrands, and determine the two-loop integrands for any number of external operators. The result is expressed as a linear combination of conformal integrals, with coefficients that are rational functions of the spacetime distances and operator polarizations. We obtain an exact match with a one-loop integrability computation, and study the near-massless limit of the pentagon function.

Contents

1	Introduction	1
2	Ten-Dimensional Null Limit	4
3	Polynomials from Generating Functions	9
3.1	The Square (a. k. a. Octagon)	10
3.2	The Pentagon	10
3.3	The Hexagon	13
4	Twistor Rules for 10d Null Polygons	14
5	All 10d Null Polygons to Two Loops	17
5.1	Factorization Channels	18
5.2	One-Loop Result	20
5.3	Two-Loop Result	20
6	Interacting 10d Null Polygons	25
6.1	Pentagon at Integrated Level	25
6.2	4d Null Polygon Limit	26
6.3	Leading Logarithms	28
7	Match with Hexagons	30
8	Discussion	31
A	Two-Loop Faces in Terms of Conformal Integrals	35
References		37

1 Introduction

Correlation functions of local operators are the most natural observables to consider in a conformal field theory. This is no different in planar $\mathcal{N} = 4$ super Yang–Mills theory, where the most studied correlation functions are those among protected single-trace operators. Supersymmetry prevents their two- and three-point functions to receive quantum corrections, their four- and higher-point functions are extremely non-trivial, and contain a wealth of information about the theory.

The four-point correlator of the lightest protected scalar operators (which are part of the stress-tensor multiplet) is known to various orders in both the weak-coupling [1, 2] and strong-coupling expansions [3–5]. Also higher-point correlators of these operators have been computed at weak [6, 7] and strong coupling [8, 9]. These observables provide access to non-protected structure constants through OPE limits [10–14], and connect to Wilson loops [15] and gluon scattering amplitudes [16–23] via light-like polygon limits and T-duality.

In this paper, we focus on the opposite regime of large-charge operators. Their correlators are particularly amenable to integrability in the form of hexagonalization [24–27]. In fact, their four-point function in the large-charge limit (in a suitable charge polarization) has been

computed to all orders in perturbation theory [28–31], and even at finite coupling [32,33]. The five-point counterpart is known to two loops in weak-coupling perturbation theory [13,34]. More structure emerges once we unify both the light and the large-charge correlators into a single common object, the so-called generating function [35,36], which encodes not only these correlators, but in fact all possible correlation functions of half-BPS scalar operators with arbitrary charges. The generating function is

$$G_n = \sum_{k_1, \dots, k_n=2}^{\infty} \langle \mathcal{O}_{k_1}(x_1, y_1) \dots \mathcal{O}_{k_n}(x_n, y_n) \rangle, \quad \mathcal{O}_k(x, y) = \frac{1}{k} \text{tr} (y \cdot \phi(x))^k, \quad (1.1)$$

where ϕ are the six scalars of the theory, and y_i are six-dimensional null polarization vectors, $y_i \cdot y_i = 0$. These generating functions have been computed at weak coupling to high orders at four points [35], and to two and one loops at five and six points, respectively [14]. They display two remarkable properties:

- After factoring out the universal four-point superinvariant, the reduced four-point generating function displays a hidden ten-dimensional conformal symmetry [35]. The same symmetry has been observed at strong values of the coupling, in the tree-level supergravity regime of the bulk dual [37,38].¹ At higher points, there is so far only limited evidence (but also no contraindication) of this symmetry [14]. Since the symmetry holds at the level of the integrands, it is yet unclear how the weak-coupling and strong-coupling instances are related. The symmetry is broken at integrated level at weak coupling, and it is broken by stringy corrections to supergravity. Hence it is not a symmetry that interpolates between weak and strong coupling, and it might not have the same origins at weak and strong coupling.
- After taking a ten-dimensional null polygon limit, the generating functions are conjecturally dual to massive scattering amplitudes on the Coulomb branch of $\mathcal{N} = 4$ super Yang–Mills theory [35,40,41].

To date, there is no first-principles derivation of the ten-dimensional symmetry. However, in the planar limit, the generating function integrands organize themselves in terms of ten-dimensional distances

$$D_{ij} = -\frac{y_{ij}^2}{X_{ij}^2}, \quad X_{ij}^2 = x_{ij}^2 + y_{ij}^2 \quad (1.2)$$

that re-sum geometric series $D_{ij} = d_{ij} + d_{ij}^2 + d_{ij}^3 + \dots$ of four-dimensional propagators $d_{ij} = -y_{ij}^2/x_{ij}^2$. In terms of these ten-dimensional distances, focusing on a correlator that has a large charge flow between points x_i and x_j ($k_i, k_j \rightarrow \infty$, with a large power of y_{ij}^2) is equivalent to taking the ten-dimensional null limit $X_{ij}^2 \rightarrow 0$ of the generating function.

Thus by taking the combined limit $X_{i,i+1}^2 \rightarrow 0$ with $i = 1, \dots, n$, one focuses on correlators where all operators have large charge, $k_i \rightarrow \infty$, and moreover the limit enforces a large charge flow between each pair of neighboring operators $i, i+1$. This is the ten-dimensional null polygon limit introduced in [35]. The most important aspect of the resulting 10d null polygon correlators is their factorization property. This can be easily understood in perturbation theory. In the free theory, the large charge flow means that every pair of neighboring operators is connected by a large number of propagators, which, due to the planar limit, all lie in parallel without crossing (in color space), forming a bundle (“ribbon”

¹A similar 8d symmetry was recently observed for correlators of 1/2 BPS operators in 4d $\mathcal{N} = 4$ SQCDs [39].

or “bridge”). These bridges cut the color sphere into two disk-like regions, an “inside” and an “outside”. For any virtual particle to couple the inside with the outside (in the planar limit), that particle must cross a large bundle of propagators, and thus such processes are suppressed by a factor g^{2k} , where g is the coupling, and k is the width of the bundle.

At the same time, virtual processes that are internal to a single propagator bundle cancel each other out due to supersymmetry, since all operators are BPS and thus have protected two-point functions. Therefore, sending the number of propagators between neighboring operators to infinity (by taking the ten-dimensional null limit) decouples the inside and the outside to all orders in perturbation theory, making the large-charge correlator factorize into the square of a simpler object, the *polygon correlator* \mathbb{M}_n :

$$\lim_{x_{i,i+1}^2 \rightarrow 0} \left(\prod_{i=1}^n \frac{X_{i,i+1}^2}{x_{i,i+1}^2} \right) N_c^{n-2} G_n = \mathbb{M}_n \times \mathbb{M}_n. \quad (1.3)$$

The simplest non-trivial polygon is the “octagon” \mathbb{M}_4 studied in [28, 29, 35]. But the limit (1.3) defines n -sided polygon correlators \mathbb{M}_n for any n , and these will be the primary objects of study in this work.

More precisely, we focus on the ℓ -loop *integrands* $M_{n,\ell}$ of the polygon correlators \mathbb{M}_n , defined via the Lagrangian insertion procedure (see (2.11) below). We explicitly compute these loop integrands at two loops in perturbation theory, by two different methods. Firstly by taking the ten-dimensional null polygon limit (1.3) of the generating functions computed in [14]. Secondly, we notice that the twistor Feynman rules devised to compute the integrands of the generating functions G_n [36] can be adapted to directly compute the polygon integrands $M_{n,\ell}$ themselves, by restricting to graphs with disk topology. The latter method allows us to compute the two-loop polygon integrands $M_{n,2}$ for up to $n = 10$ points. They are expressed in a rational basis of integrands of conformal integrals. From the data up to $n = 10$, we could derive a general formula for the coefficients of this expansion that holds for any n . We verified its correctness by comparing against the twistor computation at $n = 11$ points. Our result is available in the ancillary MATHEMATICA file `polygons.m`.

An important property of the polygon correlators are their factorization limits. This follows in the same way as the factorization of the full generating functions into the product of two polygons: Taking a ten-dimensional null limit on any diagonal of a polygon correlator focuses on a large charge flow on this diagonal, and thus factorizes the polygon into the product of two smaller polygons. The computation of any polygon is thus reduced to assembling all factorization channels from products of smaller polygons, and computing a remaining function that is free of ten-dimensional poles (see (5.1) below). We find closed-form expressions for all these pole-free functions at one and two loops (see (5.11) and (5.13) below), from which we reconstruct the two-loop integrand $M_{n,2}$ for any n -sided polygon. We also compare this decomposition with a similar expansion from integrability at one loop [42], and find complete agreement.

Finally, we consider the integration of the polygon integrands $M_{n,\ell}$ to the interacting polygon correlators \mathbb{M}_n . Unfortunately, the required conformal integrals are mostly unknown, hence our analysis is limited to five-point polygons \mathbb{M}_5 at two-loops and in nearly massless kinematics. After evaluating the contributing integrals, we find perfect agreement with the four-dimensional polygonal null limit $x_{i,i+1}^2 \rightarrow 0$ computed in [13, 41] and the leading logarithm limit (also known as “stampedes” limit) considered in [43, 44].

This work is organized as follows. In Section 2, we introduce the polygon correlators as limits of the full generating functions in ten-dimensional null kinematics, and highlight their many interesting properties. In Section 3, we compute five-point and six-point polygon integrands from the ten-dimensional null limit of the respective generating functions. In

Section 4, we explain how to compute the polygon integrands directly from the twistor Feynman rules of [36]. In Section 5, we introduce the faces decomposition, and find all polygon integrands at two loops. In Section 6, we consider the integrated polygon correlators, and compare them with previously studied near-massless limits. In Section 7, we compare the faces decomposition with a similar result from integrability, finding an exact match, and highlighting the differences between the two expansions. We conclude by discussing interesting future directions in Section 8.

2 Ten-Dimensional Null Limit

In this section, we present the higher-point generalizations of the *octagon* function [28, 29] (here renamed as *square*). These higher-point polygons are defined as the residues of the n -point generating functions on a polygonal set of ten-dimensional poles [35].

Generating Function. In $\mathcal{N} = 4$ super Yang–Mills theory, correlation functions of half-BPS scalar operators of any charges can be naturally re-packaged into correlation functions of “master” operators [35, 36]

$$\mathcal{O}(x, y) = \sum_{k=2}^{\infty} \mathcal{O}_k(x, y), \quad \mathcal{O}_k(x, y) = \frac{1}{k} \text{tr} [y \cdot \phi(x)]^k + \text{multi-traces}. \quad (2.1)$$

where ϕ are the six scalars of the theory, and the polarization vectors y_i satisfy the BPS condition

$$y \cdot y \equiv y^{AB} y_{AB} = 0 \quad \text{with} \quad A, B = 1, 2, 3, 4. \quad (2.2)$$

The operators \mathcal{O}_k have fixed R-charge k : The operator with $k = 2$ is the scalar component of the stress-tensor multiplet, which is dual to the AdS_5 graviton, and the higher- k operators are dual to the higher Kaluza–Klein modes.

Just like the correlation functions of fixed-charge operators \mathcal{O}_k , the correlator of master operators (2.1) can be written via the Lagrangian insertion procedure as

$$\left\langle \prod_{i=1}^n \mathcal{O}(x_i, y_i) \right\rangle_{\text{SYM}} = \sum_{\ell=0}^{\infty} \frac{(-g^2)^\ell}{\ell!} \int \left[\prod_{k=1}^{\ell} \frac{d^4 x_{n+k}}{\pi^2} \right] G_{n,\ell}, \quad (2.3)$$

where $G_{n,\ell}$ is the correlator of n operators \mathcal{O} and ℓ chiral interaction Lagrangian operators L_{int} :

$$G_{n,\ell} \equiv \left\langle \prod_{i=1}^n \mathcal{O}(x_i, y_i) \prod_{i=1}^{\ell} L_{\text{int}}(x_i) \right\rangle_{\text{SDYM}}. \quad (2.4)$$

where the subscript “SDYM” signifies that this correlation function is evaluated with the self-dual part of the $\mathcal{N} = 4$ SYM action (which is equivalent to evaluating the correlator at Born level in the full theory).

The correlator (2.4) by definition of the operators (2.1) serves as a generating function for the integrands of fixed-charge correlators,

$$G_{n,\ell} = \sum_{k_1, \dots, k_n=2}^{\infty} \langle k_1 \dots k_n \rangle_{\ell}, \quad (2.5)$$

where the correlators $\langle k_1 \dots k_n \rangle$ of fixed-charge operators \mathcal{O}_k can be extracted from $G_{n,\ell}$ via

$$\begin{aligned} \langle k_1 k_2 \dots k_n \rangle_{\ell} &\equiv \left\langle \prod_{i=1}^n \mathcal{O}_{k_i}(x_i, y_i) \prod_{i=1}^{\ell} L_{\text{int}}(x_i) \right\rangle_{\text{SDYM}} \\ &= \frac{1}{k_1!} \frac{\partial^{k_1}}{\partial t_1^{k_1}} \dots \frac{1}{k_n!} \frac{\partial^{k_n}}{\partial t_n^{k_n}} G_{n,\ell}(x_i, t_i y_i) \Big|_{t_i \rightarrow 0}. \end{aligned} \quad (2.6)$$

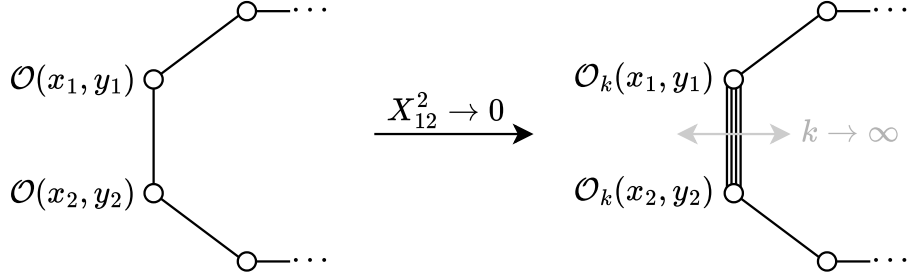


Figure 1: The ten-dimensional null limit of the generating function projects onto an infinite number of four-dimensional propagators between the two operators.

Ten-Dimensional Poles. One notable feature of the generating function (2.4) is that it is expressed in terms of ten-dimensional propagators

$$D_{ij} = -\frac{y_{ij}^2}{X_{ij}^2}, \quad X_{ij}^2 = x_{ij}^2 + y_{ij}^2, \quad (2.7)$$

where

$$x_{ij}^2 \equiv (x_i - x_j)^2, \quad y_{ij}^2 \equiv (y_i - y_j)^2 = -2 y_i \cdot y_j \quad (2.8)$$

are the four-dimensional space-time and the six dimensional R-charge distances between operators i and j . These propagators D_{ij} connect the external operators (2.1).² Expanding around $y_{ij}^2 = 0$, they become a geometric sum of arbitrary powers of ordinary four-dimensional propagators d_{ij} :

$$D_{ij} = d_{ij} + d_{ij}^2 + d_{ij}^3 + \dots, \quad d_{ij} = -\frac{y_{ij}^2}{x_{ij}^2}. \quad (2.9)$$

The component correlators (2.6) are recovered by performing this expansion and keeping only the appropriate powers of the various y_i polarizations.

Correlators of operators \mathcal{O}_k with small R-charge k receive contributions from the first terms in the series (2.9). Conversely, in the planar limit, correlators of operators with parametrically large R-charge, come from the infinite tail of the geometric series. This can be understood by noting that the Feynman rules only admit propagators D_{ij} that are homotopically distinct from each other on the color sphere [36]. For a finite number of operators, only finitely many such propagators can be drawn on the color sphere. To accommodate for large-charge operators, at least some of the propagators D_{ij} must thus be expanded to large orders. As already noted in [35], one can focus on such large-charge correlators directly at the level of the generating function (2.5) by taking the ten-dimensional null limit: $X_{ij}^2 \rightarrow 0$ (or equivalently $d_{ij} \rightarrow 1$). By considering this limit, we project the generating function to correlators where an infinite number of parallel four-dimensional propagators d_{ij} connect the operators at points x_i and x_j , as depicted in Figure 1.

Polygons. A particularly interesting limit is the *ten-dimensional null polygon limit*, in which we simultaneously take $X_{i,i+1}^2 \rightarrow 0$, $i = 1, \dots, n$, such that the n operators (2.1) sit at

²The correlator (2.4) is a component of a parent supercorrelator of $n + \ell$ superoperators \mathbb{O} , in which all propagators take the ten-dimensional form (2.7), see [36]. The component is recovered by a superprojection and the limit $y_i \rightarrow 0$, $i = n + 1, \dots, \ell$, which demotes all propagators that connect to Lagrangian operators L_{int} to ordinary four-dimensional form d_{ij} .

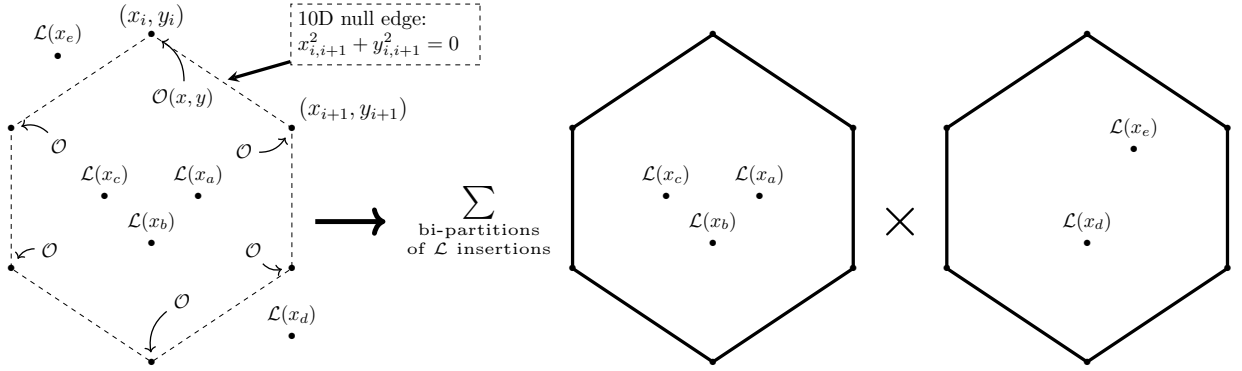


Figure 2: The ten-dimensional null polygon limit factorizes the correlator into two polygons.

the cusps of an n -sided polygon, where the edges are “thick” propagators of large (essentially infinite) R-charge that connect neighboring operators. This thick propagator perimeter drastically simplifies the correlator, since the “inside” and the “outside” of the perimeter decouple to all orders in perturbation theory. The correlator thus factorizes into the product of two simpler disk-like objects [35], the *polygons* $M_{n,\ell}$:

$$\lim_{\substack{d_{i,i+1} \rightarrow 1 \\ i=1, \dots, n}} \prod_{i=1}^n (1 - d_{i,i+1}) \times N_c^{n-2} G_{n,\ell} = \sum_{\mathbf{k}} M_{n,\mathbf{k}} \times M_{n,\bar{\mathbf{k}}} \quad (2.10)$$

where the factor N_c^{n-2} is chosen such that $M_{n,\mathbf{k}} \sim N_c^0$, and the sum on the right-hand side runs over all possible ways of distributing the ℓ Lagrangians onto the two polygons: $\mathbf{k} \cup \bar{\mathbf{k}} = \{n+1, \dots, n+\ell\}$. Thus, the n -point polygons $M_{n,\mathbf{k}}$ are correlators with disk topology, with n large-charge operators inserted at the boundary of the disk, and the set \mathbf{k} of Lagrangian operators inserted in the interior, see Figure 2. In the case where all Lagrangians are inserted in a single polygon, $\mathbf{k} = \{n+1, \dots, n+\ell\}$, we use the simplified notation $M_{n,\mathbf{k}} \equiv M_{n,\ell}$. These polygons $M_{n,\ell}$ define the integrands of the n -point interacting polygon correlator

$$\mathbb{M}_n = \sum_{\ell=0}^{\infty} \frac{(-g^2)^\ell}{\ell!} \int \left[\prod_{k=1}^{\ell} \frac{d^4 x_{n+k}}{\pi^2} \right] M_{n,\ell}. \quad (2.11)$$

Using (2.3), the factorization (2.10) can be written at integrated level as:

$$\lim_{\substack{d_{i,i+1} \rightarrow 0 \\ i=1, \dots, n}} \prod_{i=1}^n (1 - d_{i,i+1}) \times N_c^{n-2} \left\langle \prod_{i=1}^n \mathcal{O}(x_i, y_i) \right\rangle_{\text{SYM}} = \mathbb{M}_n \times \mathbb{M}_n. \quad (2.12)$$

The four-point and five-point polygons \mathbb{M}_4 and \mathbb{M}_5 have been conventionally called *octagon* and *decagon* in the literature. The origin of these names lies in their integrability-based description in terms of hexagon form factors [24, 25], in which the cusps acquire a non-zero “length”. In this work, we will call these objects *square* and *pentagon*, respectively, and consider their higher-point counterparts.

The polygon correlators $M_{n,\ell}$ and \mathbb{M}_n satisfy several interesting properties:

Factorization. Upon taking additional ten-dimensional null limits on their diagonals, the polygons $M_{n,\ell}$ factorize into lower-point polygons:

$$\lim_{d_{ij} \rightarrow 0} (1 - d_{ij}) M_{n,\ell} = \sum_{\mathbf{k}} M_{\mathbf{m},\mathbf{k}} \times M_{\bar{\mathbf{m}},\bar{\mathbf{k}}}, \quad (2.13)$$

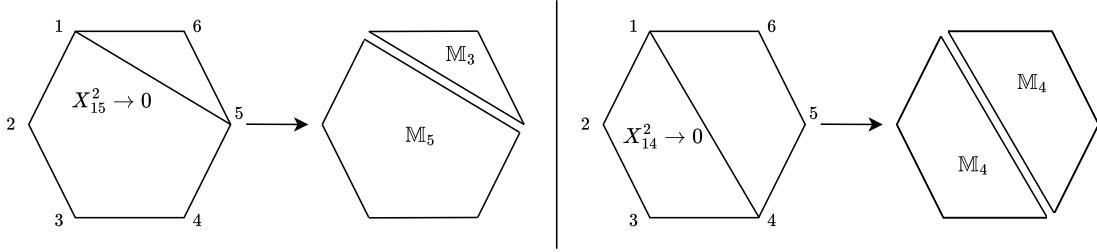


Figure 3: Factorization of the hexagon into lower polygons after taking ten-dimensional null limits on the diagonals.

where $\mathbf{m} = \{i, \dots, j \pmod n\}$ and $\bar{\mathbf{m}} = \{j, \dots, i \pmod n\}$ are the external operators “left” and “right” of the line (i, j) , and the sum runs over all bipartitions $\mathbf{k} \dot{\cup} \bar{\mathbf{k}} = \{n+1, \dots, n+\ell\}$ of the Lagrangian insertion points onto the two factors. Here, we employ the slight abuse of notation $M_{\mathbf{m}, \mathbf{k}} = M_{|\mathbf{m}|, \mathbf{k}}$ with point labels \mathbf{m} . For example, the following limit splits the two-loop pentagon $M_{5,2}$ into a square and a triangle:

$$\lim_{d_{14} \rightarrow 0} (1 - d_{14}) M_{5,2} = M_{\mathbf{m}, \emptyset} M_{\bar{\mathbf{m}}, \{6,7\}} + M_{\mathbf{m}, \{6\}} M_{\bar{\mathbf{m}}, \{7\}} + M_{\mathbf{m}, \{7\}} M_{\bar{\mathbf{m}}, \{6\}} + M_{\mathbf{m}, \{6,7\}} M_{\bar{\mathbf{m}}, \emptyset} \quad (2.14)$$

with $\mathbf{m} = \{1, 2, 3, 4\}$ and $\bar{\mathbf{m}} = \{1, 4, 5\}$. See Figure 3 for an illustration. The factorization (2.13) follows by the same reasoning as the factorization of the generating function $G_{n,\ell}$ into two polygon factors (2.10): Taking the $X_{ij}^2 \rightarrow 0$ limit projects to the tail of the geometric series (2.9), thus it limits to terms that include a parametrically large number of parallel propagators d_{ij} that separates the polygon into two subregions that do not interact with each other. The factorization straightforwardly lifts to the integrated polygons:

$$\lim_{d_{ij} \rightarrow 0} (1 - d_{ij}) \mathbb{M}_n = \mathbb{M}_{\mathbf{m}} \times \mathbb{M}_{\bar{\mathbf{m}}}, \quad (2.15)$$

with \mathbf{m} and $\bar{\mathbf{m}}$ as in (2.13).

No Double Poles. The generating function $G_{n,\ell}$ in general contains double and higher poles in the ten-dimensional distances X_{ij}^2 . These originate in Feynman graphs where external operators i and j are connected by multiple homotopically distinct propagators D_{ij} . In order to be homotopically distinct, any two such propagators connecting the same two operators must enclose at least one third operator.³ The polygon disk-topology excludes such diagrams, and thus the polygon correlators $M_{n,\ell}$ only contain at most simple poles in the ten-dimensional distances X_{ij}^2 .

Direct Computability. As we will see below in Section 4, the polygons $M_{n,\ell}$ can be computed directly from the twistor Feynman rules of [36], avoiding the computation (and subsequent ten-dimensional polygon limit) of the much more complicated generating functions $G_{n,\ell}$ altogether.

Massive Amplitudes. There is a well-established duality in $\mathcal{N} = 4$ super Yang–Mills that relates the four-dimensional null polygon limit $x_{i,i+1}^2 \rightarrow 0$ of the n -point correlation function of the lightest half-BPS operators, $k_i = 2$ in (2.5), with the n -point *massless* MHV gluon scattering amplitude [15, 21–23, 45–48]. A less firmly established duality,

³Two propagators D_{ij} are also homotopically distinct if they only enclose Lagrangian operators, but no further external operators. Such terms however evaluate to zero, which is in accordance with the fact that two-point functions of scalar BPS operators are protected from quantum corrections.

but with corroborating evidence in the case of four [35] and five points [40, 41], is that something similar also happens in the large R-charge limit. The statement is that the n -point polygons \mathbb{M}_n are dual to *massive* n -point W-boson scattering amplitudes on the Coulomb branch of $\mathcal{N} = 4$ super Yang–Mills theory [35]. Upon additionally taking the *massless* null polygon limit $x_{i,i+1}^2 \rightarrow 0$, these further reduce to the massless MHV gluon amplitudes.

More precisely, the polygons $M_{n,\ell}$ reduce to the ℓ -loop integrands $\mathcal{A}_{n,\ell}$ of the *massless* MHV scattering amplitudes when one sets all internal diagonals d_{ij} to zero and passes to the four-dimensional null limit:

$$M_{n,\ell} \rightarrow \mathcal{A}_{n,\ell}/\mathcal{A}_{n,0} \quad \text{for} \quad x_{i,i+1}^2 \rightarrow 0, \quad i = 1, \dots, n \quad \text{and} \quad d_{ij} \rightarrow 0 \quad \forall i, j, \quad (2.16)$$

where $\mathcal{A}_{n,\ell}$ is the ℓ -loop massless MHV amplitude integrand, and $\mathcal{A}_{n,0}$ its tree-level expression. The relation (2.16) follows by construction when both the amplitude integrands $\mathcal{A}_{n,\ell}$ and the polygons $M_{n,\ell}$ are computed from Lagrangian insertions, see e. g. [46, 47]. The limit can simply be achieved by setting all y_{ij}^2 to zero, noticing that $x_{i,i+1}^2 = -y_{i,i+1}^2 \rightarrow 0$ on the perimeter of the polygon, due to the ten-dimensional null limit $0 = X_{i,i+1}^2 = x_{i,i+1}^2 + y_{i,i+1}^2$.

Integrability. The polygons \mathbb{M}_n are the most natural objects to be computed from integrability via hexagonalization, i. e. decomposition into hexagon form factors [24–26]. Due to their disk topology, they are free of mirror excitations that wrap operator insertions that require careful treatment [49]. The polygon configurations in fact make hexagonalization conceptionally very similar to the pentagon OPE for massless amplitudes (null polygon Wilson loops) [50–53], and in the four-dimensional null limit, the two should become equivalent. In the case of the square (a. k. a. octagon), the simplifications of the ten-dimensional null limit enabled its bootstrap to all loops [29–31], and a finite-coupling resummation in terms of a Fredholm determinant [32, 33]. The pentagon (a. k. a. decagon) has been computed to two loops [34]. Also more general correlators become most computable in limits where they can be decomposed into polygons [54], even at subleading non-planar orders of the planar limit expansion [42, 55].

Relation with Fixed-Charge Correlators. The full generating function $G_{n,\ell}$ contains the complete information on all fixed-charge correlators via (2.6). Since the ten-dimensional null polygon limit captures only a specific part of the generating function, it also only contains partial information on any given fixed-charge correlator. Without involving the full generating function, any single generic fixed-charge correlator cannot easily be projected to the part captured by polygons. An exception to this are certain correlators at four, five, and six points, where one can engineer specific operators of large (but fixed) charge, such that the correlator equals the square, pentagon, or hexagon, up to a loop order that is bounded by the operator charges. The operators are R-symmetry descendants of the fixed-charge operators \mathcal{O}_k (2.1), designed so that they form a square/pentagon/hexagon, where only neighboring operators can contract with free propagators. This is how the square was originally defined [28] (see also [54], in particular Figure 11 there).

Since $\mathcal{N} = 4$ super Yang–Mills has only six scalars that transform in the $\text{SO}(6)$ R-symmetry, this procedure only works up to six points. Beyond six points, there is not enough space in the $\text{SO}(6)$ to ensure large propagator bundles between neighboring operators. Therefore, any higher-point function with sufficiently large charges will have contributions that factorize into polygons, but will also have other contributions that do not factorize, as exemplified in Figure 4.

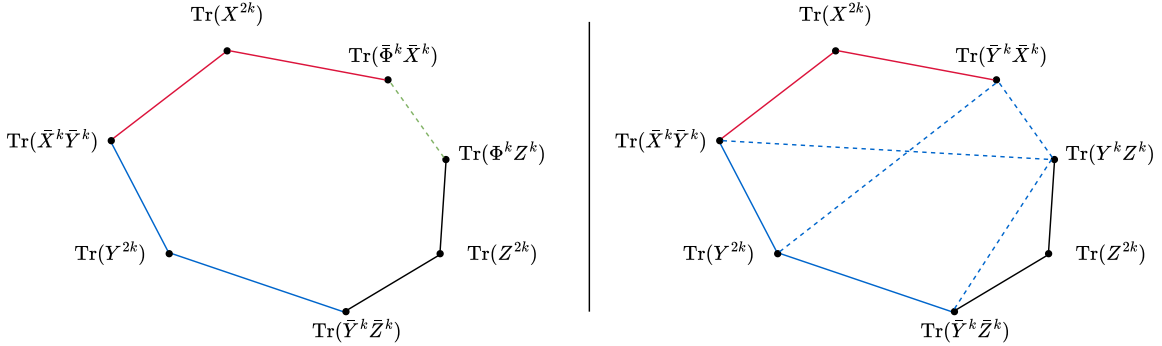


Figure 4: Seven point correlation functions of large charge operators. On the left what one would like to engineer with a field Φ so that the correlator is given by a thick perimeter and factorizes into two heptagons. There is no choice of fields $\Phi = \{X, \bar{X}, Z, \bar{Z}, Y, \bar{Y}\}$ that results into this single configuration. As example, on the right we have the case of $\Phi = Y$ where one has to sum over all the possible ways of distributing the $Y\bar{Y}$ propagators (blue), only one of these configurations will be factored out in the product of two heptagons.

Even though there is no one-to-one map between polygons and large-charge correlators beyond six points, these polygons are interesting objects on their own — as corroborated by their properties listed above; in particular their identification as massive amplitudes and their particularly nice integrability representation in terms of hexagon form factors. Computing these objects in perturbation theory is the first step towards better understanding them and it is what we turn to next.

3 Polygons from Generating Functions

Before addressing their direct construction from twistor Feynman rules, we will compute the first few one-loop and two-loop polygons by taking the ten-dimensional null limits (2.10) of the generating functions $G_{n,\ell}$ determined in [14, 36]. To this end, we first define the null polygon residue

$$R_{n,\ell} \equiv \underset{\substack{d_{i,i+1}=1 \\ i=1,\dots,n}}{\text{Res}} N_c^{n-2} G_{n,\ell} = \lim_{d_{i,i+1} \rightarrow 1} \prod_{i=1}^n (1 - d_{i,i+1}) \times N_c^{n-2} G_{n,\ell} \quad (3.1)$$

Looking at (2.10), one can see that the polygons $M_{n,\ell}$ can be determined from $R_{n,\ell}$ loop order by loop order. Explicitly:

$$M_{n,0} = (R_{n,0})^{1/2}, \quad M_{n,1} = \frac{R_{n,1}}{2 M_{n,0}}, \quad M_{n,2} = \frac{R_{n,2} - 2 (M_{n,1})^2}{2 M_{n,0}}, \quad \dots \quad (3.2)$$

The simplest polygon is the triangle. Since three-point functions of half-BPS scalar operators are protected from quantum corrections, the generating function is simply given by its leading-order term $G_{3,0} = D_{12}D_{13}D_{23}$, and therefore the triangle correlator is trivial:

$$\mathbb{M}_3 = M_{3,0} = 1. \quad (3.3)$$

3.1 The Square (a. k. a. Octagon)

Both the four-point generating function $G_{n,\ell}$ and its ten-dimensional null polygon limit were computed in [35]. Collecting the results, the square correlator reads

$$\begin{aligned} M_{4,0} &= \frac{x_{13}^2 x_{24}^2 - y_{13}^2 y_{24}^2}{X_{13}^2 X_{24}^2}, \\ M_{4,1} &= M_{4,0} \frac{X_{13}^2 X_{24}^2}{X_{15}^2 X_{25}^2 X_{35}^2 X_{45}^2} \Big|_{y_5 \rightarrow 0}, \\ M_{4,2} &= M_{4,0} \frac{X_{13}^2 X_{24}^4 X_{15}^2 X_{36}^2 + X_{13}^4 X_{24}^2 X_{45}^2 X_{26}^2 + (X_5 \leftrightarrow X_6)}{(X_{15}^2 X_{25}^2 X_{35}^2 X_{45}^2) X_{56}^2 (X_{16}^2 X_{26}^2 X_{36}^2 X_{46}^2)} \Big|_{y_5, y_6 \rightarrow 0} \end{aligned} \quad (3.4)$$

Before taking the $y_5, y_6 \rightarrow 0$ limits, these functions include the dependence on all higher Kaluza–Klein modes of the Lagrangian operator. Written in this form, the ratios $M_{4,\ell}/M_{4,0}$ display a 10D (dual) conformal symmetry, which only gets broken by taking the $y_i \rightarrow 0$ limit to project to the chiral interaction Lagrangian $L_{\text{int}}(x)$. It corresponds to the loop-integrand in higher-dimensional SYM, and by dimensional reduction gives the integrand of a massive amplitude on the Coulomb branch [35].

Performing the $y_5, y_6 \rightarrow 0$ projection, the square correlator can alternatively be expanded in a basis of integrands of conformal integrals:⁴

$$M_{4,0} = \frac{1 - d_{13}d_{24}}{(1 - d_{13})(1 - d_{24})}, \quad (3.5)$$

$$M_{4,1} = (1 - d_{13}d_{24})x_{13}^2 x_{24}^2 B^{[1,2,3,4;5]}, \quad (3.6)$$

$$M_{4,2} = (1 - d_{13}d_{24})x_{13}^2 x_{24}^2 \left[\mathcal{I}_5^{[1,3|2,4;5,6]} X_{13}^2 + \mathcal{I}_5^{[2,4|1,3;5,6]} X_{24}^2 \right], \quad (3.7)$$

where (see also Figure 5)

$$B^{[1,2,3,4;a]} = \frac{1}{x_{1a}^2 x_{2a}^2 x_{3a}^2 x_{4a}^2}, \quad (3.8)$$

$$\mathcal{I}_5^{[1,2|3,4;a,b]} = \frac{1}{(x_{1a}^2 x_{2a}^2 x_{3a}^2) x_{ab}^2 (x_{1b}^2 x_{2b}^2 x_{4b}^2)} + (a \leftrightarrow b). \quad (3.9)$$

Note that the square correlators $M_{4,\ell}$, $\ell > 0$ take the form of a universal prefactor $(1 - d_{13}d_{24})x_{13}^2 x_{24}^2$, multiplied by a combination of conformal integrands with ten-dimensional coefficients. This form follows from the ten-dimensional nature of the parent expressions (3.4), and it continues at higher loop orders. The prefactor $(1 - d_{13}d_{24})x_{13}^2 x_{24}^2$ in fact originates from the null polygon limit of the universal four-point supersymmetry invariant R_{1234} that appears as an overall factor in the four-point generating function [1]: $G_{4,\ell} = R_{1234} \mathcal{H}_{4,\ell}$, with $\mathcal{H}_{4,\ell}$ the reduced correlator [35]:

$$\lim_{d_{i,i+1} \rightarrow 1} R_{1234} = (1 - d_{13}d_{24})^2 x_{13}^2 x_{24}^2. \quad (3.10)$$

3.2 The Pentagon

Using the the five-point generating functions provided in [14] (see (6.16) and (6.19) there), we compute the one-loop and two-loop pentagon by applying (3.1) and (3.2):⁴

$$M_{5,0} = \frac{1}{5} + \frac{d_{13}}{(1 - d_{13})(1 - d_{14})} + (\text{C}_5 \text{ perms}) \quad (3.11)$$

⁴The labels \mathcal{I}_5 , \mathcal{I}_6 , and \mathcal{I}_7 for the conformal integrals displayed in (3.6)–(3.15) are inherited from [14].

$$M_{5,1} = \frac{p_{1234}}{2} B^{[1,2,3,4;6]} - 2i \mathcal{I}_{\text{odd}}^{[1,2,3,4;6]} + (\text{C}_5 \text{ perms}), \quad (3.12)$$

$$\begin{aligned} M_{5,2}^{\text{even}} &= \frac{p_{1234}}{2} \left(\mathcal{I}_5^{[1,3|2,4;6,7]} X_{13}^2 + \mathcal{I}_5^{[2,4|1,3;6,7]} X_{24}^2 + \mathcal{I}_6^{[1,4|2,3|5;6,7]} X_{14}^2 \right) \\ &+ \frac{X_{35}^2 q_{12345} + X_{13}^2 q_{54321}}{2} \mathcal{I}_7^{[1,2|4,5|3;6,7]} + (\text{C}_5 \text{ perms}), \end{aligned} \quad (3.13)$$

The two-loop pentagon is restricted to its parity-even part. The parity-odd part of the one-loop pentagon is written as a sum of four-point parity-odd integrands

$$\mathcal{I}_{\text{odd}}^{[1,2,3,4;0]} = \frac{\epsilon_{\mu\nu\rho\sigma} x_{10}^\mu x_{30}^\nu x_{30}^\rho x_{40}^\sigma}{x_{10}^2 x_{20}^2 x_{30}^2 x_{40}^2}, \quad (3.14)$$

and we introduce the following conformal integrals for the two-loop pentagon (see [Figure 5](#))

$$\begin{aligned} \mathcal{I}_6^{[1,2|3,4|5;a,b]} &= \frac{x_{5a}^2}{(x_{1a}^2 x_{2a}^2 x_{3a}^2 x_{4a}^2) x_{ab}^2 (x_{1b}^2 x_{2b}^2 x_{5b}^2)} + (a \leftrightarrow b), \\ \mathcal{I}_7^{[1,2|3,4|5;a,b]} &= \frac{1}{(x_{3a}^2 x_{4a}^2 x_{5a}^2) x_{ab}^2 (x_{1b}^2 x_{2b}^2 x_{5b}^2)} + (a \leftrightarrow b). \end{aligned} \quad (3.15)$$

The result (3.13) for the two-loop pentagon $M_{5,2}$ is consistent with the known expressions for the “decagon” function [13, 34].

Similar to the case of the square, one can see that the pentagon expressions at one and two loops are written in terms of four-dimensional structures p and q that multiply linear combinations of conformal integrals with ten-dimensional coefficients. The four-dimensional structures are

$$p_{1234} = x_{12}^2 x_{34}^2 - x_{14}^2 x_{23}^2 + \frac{(1 + d_{14} - 2d_{13}d_{24})}{1 - d_{14}} x_{13}^2 x_{24}^2, \quad (3.16)$$

$$q_{12345} = x_{12}^2 x_{34}^2 - x_{14}^2 x_{23}^2 - \frac{d_{35}(1 - d_{13}d_{24})}{1 - d_{35}} x_{13}^2 x_{24}^2. \quad (3.17)$$

The interpretation of these structures is that they are polygon limits of components of superconformal invariants that occur in the five-point generating functions, similar to (3.10) at four points. This picture is further supported by the fact that p can be traced back to the invariants \mathcal{R}_{1234} and $\mathcal{R}_{1234,5}$ that appear in the five-point generating function as follows:⁵

$$\text{Res}_{d_{i,i+1}=1} \frac{\mathcal{R}_{1234,5} - C_{1234;5}^{(5)} \mathcal{R}_{1234}}{\prod_{i < j=1}^5 w_{ij}} = M_{5,0} \times p_{1234}, \quad (3.18)$$

where \mathcal{R}_{1234} , $\mathcal{R}_{1234,5}$, and $C_{1234;5}^{(5)}$ are given in (5.4), (6.14), and (6.12) of [14].

While the four-point generating functions $G_{4,\ell}$ are purely parity-even, the higher-point generating functions develop parity-odd parts, which also induce parity-odd parts for the respective polygons. Since the parity-odd parts integrate to zero, one might be tempted to ignore them. However, when one takes products of polygons to re-construct the null polygon correlators as in (2.10), products of parity-odd parts are essential, as they contribute to the parity-even part of the correlator. In other words, the factorization (2.10) is only consistent if one includes the parity-odd parts of both the generating functions $G_{n,\ell}$ and the polygons $M_{n,\ell}$. The parity-odd parts are similarly essential for the factorization formula (2.13).

⁵At one loop, the combination (3.18) is apparent in (6.16) of [14]. At two loops, it appears more subtly in (6.21) when dressing the integral \mathcal{I}_5 with f_5 given in (6.24).

With the expressions above, we can explicitly verify the factorization formula (2.13): Taking the ten-dimensional null limit of the diagonal $X_{14}^2 \rightarrow 0$ (or equivalently $d_{14} \rightarrow 1$ in terms of the four-dimensional propagator), the pentagon factorizes into a square and a (trivial) triangle

$$\text{Res}_{d_{14}=1} M_{5,\ell} = M_{4,\ell} \times M_{3,0} = M_{4,\ell} \times 1, \quad \ell = 0, 1, 2, \quad (3.19)$$

at leading order, one-loop, and two-loop order. Consistently, the parity-odd part of the one-loop pentagon vanishes in this limit. Notice that the poles in p and q in the two-loop pentagon are canceled by the factors X_{ij}^2 dressing the penta-box integral \mathcal{I}_6 and the five-point double-box \mathcal{I}_7 , whereas the poles of p are still present for the four-point box \mathcal{I}_5 , thus one can see that \mathcal{I}_6 , \mathcal{I}_7 , and q do not contribute to the limit (3.19).

Before moving on to the hexagon, in the following we provide some more details on the derivation of the pentagon from the generating function.

One Loop. At five points and one loop, a more general correlator than $G_{5,1}$ has been computed [14, 36]: The generating function $\tilde{G}_{5,1}$ that also includes all higher-R-charge components of the chiral Lagrangian operator (see (6.11) in [14] for the expression). The correlator $G_{5,1}$ (2.4) is obtained from $\tilde{G}_{5,1}$ by taking the $y_6 \rightarrow 0$ limit. Applying the 10d null polygonal limit (3.1), the generating function factorizes according to (2.10) and (3.1), $\tilde{R}_{5,1} = 2M_{5,0}\tilde{M}_{5,1}$, where $\tilde{M}_{5,1}$ is a generalized one-loop pentagon that includes all higher-R-charge components of the chiral Lagrangian:

$$\begin{aligned} \tilde{M}_{5,1} = & \frac{X_{56}^2 p_{1234} + d_{56}x_{56}^2 \left((1 - d_{13}d_{24})x_{13}^2 x_{24}^2 - (1 - d_{14})x_{14}^2 x_{23}^2 \right) + (\text{C}_5 \text{ perms})}{2 X_{16}^2 X_{26}^2 X_{36}^2 X_{46}^2 X_{56}^2} \\ & - \frac{4i \left[X_{123456}^{\text{anti}} - Y_{123456}^{\text{anti}} \right]_{\text{10d null}}}{X_{16}^2 X_{26}^2 X_{36}^2 X_{46}^2 X_{56}^2}, \end{aligned} \quad (3.20)$$

with p_{1234} given in (3.16). X^{anti} and Y^{anti} are antisymmetric scalars that can be defined using the six-dimensional projective vectors X^I and Y^I , which transform in the fundamental representation of the conformal group $\text{SO}(2, 4)$ and R-symmetry group $\text{SO}(6)$, respectively:

$$\begin{aligned} X_{123456}^{\text{anti}} &= \varepsilon_{IJKLMP} X_1^I X_2^J X_3^K X_4^L X_5^M X_6^P, \\ Y_{123456}^{\text{anti}} &= \varepsilon_{IJKLMP} Y_1^I Y_2^J Y_3^K Y_4^L Y_5^M Y_6^P. \end{aligned} \quad (3.21)$$

The subscript ‘‘10d null’’ in the above equation indicates that the X^I and Y^I vectors are not independent, but satisfy the 10d null constraint on the boundary of the pentagon: $X_i^I X_{i+1}^I - Y_i^I Y_{i+1}^I = 0$.

By setting $y_6 = 0$, we project out all higher-R-charge partners of the Lagrangian, and thus, obtain the loop-integrand of the pentagon at one-loop order (3.12). The scalar Y_{12345}^{anti} projects to zero, and the antisymmetric X -scalar becomes the parity-odd integral (3.14),

$$X_{123456}^{\text{anti}} = \frac{1}{2} x_{16}^2 x_{26}^2 x_{36}^2 x_{46}^2 x_{56}^2 I_{\text{odd}}^{[1,2,3,4;6]} + (\text{C}_5 \text{ perms}). \quad (3.22)$$

Two Loops. Obtaining the two-loop pentagon using the last equation in (3.2) requires a careful treatment of the parity-even and -odd parts in the one-loop pentagon. Starting from the parity-even part of five-point two-loop generating function, we compute the parity-even two-loop pentagon via

$$M_{5,2}^{\text{even}} = \frac{R_{5,2}^{\text{even}} - 2(M_{5,1}^{\text{even}})^2 + 2(M_{5,1}^{\text{odd}})^2}{2 M_{5,0}}. \quad (3.23)$$

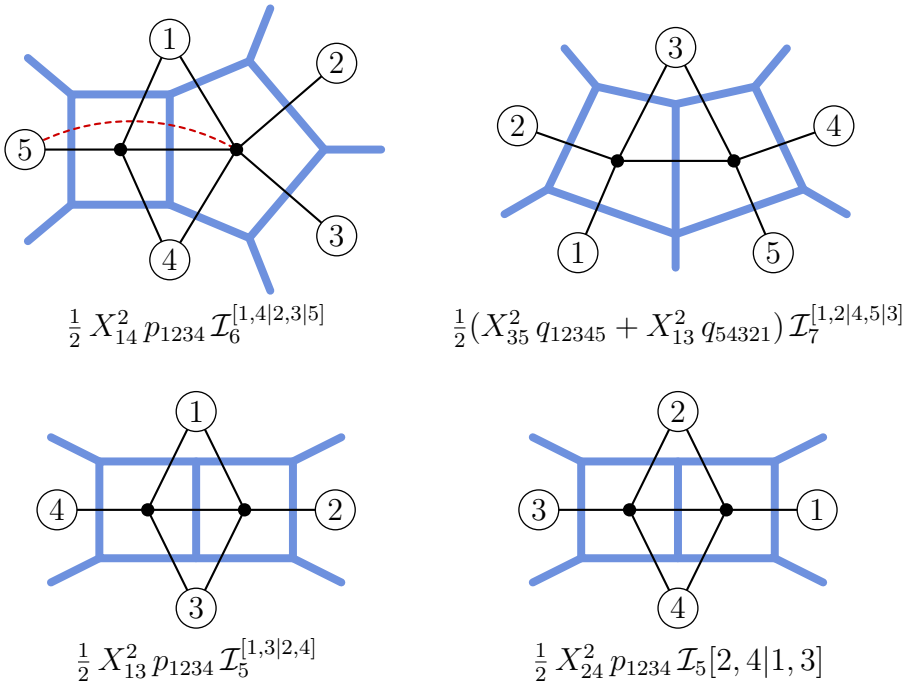


Figure 5: Conformal integrals that appear in the two-loop pentagon $M_{5,2}^{\text{even}}$, including their coefficient functions. On the first row, we present genuine five-point integrals, the second row shows the two instances of the four-point double-box. The definitions of the integrals are in (3.9), (3.15), and the factors p_{1234} and q_{12345} are defined in (3.16), (3.17). Taking an extra residue, only the the four-point integrals survive, and the pentagon $M_{5,2}^{\text{even}}$ descends to the square $M_{4,2}$ (3.19).

The parity-odd part of the one-loop pentagon squared yields an even contribution to the residue $R_{5,2}^{\text{even}}$ that needs to be subtracted in order to obtain the two-loop pentagon. Since $M_{5,1}^{\text{odd}}$ vanishes upon integration of x_6 , its contribution to (3.23) can also be omitted after lifting the expression to the integrated level. In this case, however, an integral identity has to be applied, which is exactly given by $(M_{5,1}^{\text{odd}})^2 = 0$ (after integration). In fact, this integral identity is a generalization of (6.23) in [23], where it was found in the context of the correlator/amplitude duality in the 4d null limit, where $x_{i,i+1}^2 = 0$.

Plugging the generating function $G_{5,2}$, provided in (6.19) in [14], into (3.23), we obtain the parity-even two-loop pentagon (3.13). Graphically, we depict this expression in terms of the conformal integrals (3.9) and (3.15) in Figure 5.

3.3 The Hexagon

Taking the parity-even part of one-loop six-point generating function (cf. (7.1) in [14]), we consider its 10d null hexagon limit and apply (3.2) to find the parity-even part of the one-loop hexagon⁶

$$M_{6,1}^{\text{even}} = \frac{(1 - d_{15}d_{24})}{4(1 - d_{15})(1 - d_{24})} \left(x_{12}^2 x_{45}^2 - x_{15}^2 x_{24}^2 + \frac{(1 + d_{15}d_{24} - 2d_{14}d_{25})}{1 - d_{15}d_{24}} x_{14}^2 x_{25}^2 \right) B^{[1,2,4,5;7]} - \frac{(d_{15} - d_{35})}{2(1 - d_{15})(1 - d_{35})} \left(x_{12}^2 x_{35}^2 - x_{15}^2 x_{23}^2 - \frac{(d_{15} + d_{35} - 2d_{13}d_{25})}{d_{15} - d_{35}} x_{13}^2 x_{25}^2 \right) B^{[1,2,3,5;7]}$$

⁶For the full expressions of all one-loop polygons, that include both the parity-even as well as the parity-odd parts, we refer to Section 5.2.

$$+ \frac{(1 - d_{15}d_{46})}{2(1 - d_{15})(1 - d_{46})} p_{1234} B^{[1,2,3,4;7]} + (\text{C}_6 \text{ perms}) . \quad (3.24)$$

We present the hexagon in terms of one-loop box integrals (3.8), and notice the appearance of p_{1234} that we already encountered previously in the one- and two-loop pentagon.

We verify the factorization of the hexagon into lower-point polygons by taking the following residues (see Figure 3 for illustrations of these two limits):

$$\begin{aligned} \text{Res}_{d_{15}=1} M_{6,1}^{\text{even}} &= M_{5,1}^{\text{even}} \times 1, \\ \text{Res}_{d_{36}=1} M_{6,1}^{\text{even}} &= M_{\{1236\},0} \times M_{\{3456\},1} + M_{\{1236\},1} \times M_{\{3456\},0}, \end{aligned} \quad (3.25)$$

where we recover the one-loop pentagon (3.12) (multiplying the trivial triangle) and products of the one-loop square (3.6) (with different point labels).

The explicit computations carried out in this section verify the two types of factorizations we considered: The factorization of the generating function into a product of polygons (2.10), (2.12), and the factorization of polygons into products of smaller polygons (2.13), (2.15). Although straightforward, first evaluating the full generating function to then take its ten-dimensional null polygon limit to factorize it into polygons appears like a long detour. The generating function contains much more information than the polygons, and its computation is accordingly demanding. The polygons have disk topology and contain much less information, hence there should be an easier way to compute them. Indeed it turns out there is a way to compute them directly, which is what we turn to next.

4 Twistor Rules for 10d Null Polygons

So far, we computed polygons $M_{n,\ell}$ by taking the square root of a 10d null polygonal limit $X_{i,i+1}^2 \rightarrow 0$, $i = 1, \dots, n$, of the corresponding generating function $G_{n,\ell}$. Deriving the generating function using the twistor formulation, however, is computationally quite demanding as both the number of graphs as well as the size of the ansatz grows quickly for higher points and/or higher loops.

The full generating function $G_{n,\ell}$ contains information of all underlying fixed-weight correlators, whereas the polygons only correspond to a specifically polarized large-charge limit. Hence, computing the polygons directly – without having to take a detour deriving the generating function – should be significantly more efficient. In fact, it is possible to compute the polygons directly in the twistor formalism, using the same Feynman rules as for the generating function, but restricting the choice of graphs and applying appropriate kinematics.

Prescription. To compute the full generating function $G_{n,\ell}$ in twistor space, one has to sum over all planar diagrams, i. e. graphs with sphere topology. Once we take the ten-dimensional null polygon limit, the generating function gets projected to a configuration of large-charge operators that factorizes into two polygons — in color space, the sphere factorizes to two disks, and accordingly the polygons have disk topology. It turns out that this can be directly implemented at the level of the twistor Feynman rules: The polygons $M_{n,\ell}$ can be computed directly by only considering a much smaller set of graphs $\Gamma_{n,\ell}^{\text{disk}}$, which consists of all planar graphs with disk topology whose perimeter is formed by n external operators (2.1), with two adjacent operators being connected by a single fat propagator. On the inside of the disk, ℓ Lagrangian insertions are placed that are connected by edges to each other and the

$\ell \setminus n$	4	5	6	7	8	9	10	11
0	2	3	11	29	122	479	2 113	9 369
1	9	36	176	830	4 125	20 632	104 924	538 746
2	135	740	4 203	23 273	130 113	726 250	4 069 167	22 838 831
3	2 683	17 210	106 904					
4	61 395	425 819						

Table 1: Counting of single-particle twistor graphs with disk topology for various number of external points n and internal insertions ℓ . These are ribbon (or fat) graphs with n external vertices forming the perimeter of an n -sided polygon, and ℓ internal vertices located inside the disk. The perimeter consists of simple edges, and only graphs that are inequivalent under $C_n \times S_\ell$ permutations of the vertices are counted as distinct. The first line ($\ell = 0$) counts the number of dissections of the n -gon by diagonals, see OEIS Sequence A003455.

external operators while preserving planarity. We list the counting of these graphs in Table 1. This should be contrasted with Table 1 in [14]. For example at seven points and two loops, 1 323 096 graphs contribute to the sphere generating function $G_{7,2}$, whereas the polygon $M_{7,2}$ can be computed from only 23 273 graphs. After applying the twistor Feynman rules Φ to all disk-topology graphs, one obtains the polygon $M_{n,\ell}$:⁷

$$M_{n,\ell} = \lim_{d_{i,i+1} \rightarrow 1} \prod_{i=1}^n (1 - d_{i,i+1}) \times \sum_{\gamma \in \Gamma_{n,\ell}^{\text{disk}}} \Phi(\gamma). \quad (4.1)$$

The limit manifests the 10d null polygonal kinematics that defines the polygons in the first place. It can be readily implemented when evaluating the twistor expression numerically by choosing 10d null kinematics with $X_{i,i+1}^2 = 0$.

Derivation. The reasoning for considering only graphs with disk topology is as follows: On the level of graphs, the generating function $G_{n,\ell}$ can be understood as a sum of planar ribbon graphs whose $(n + \ell)$ vertices are at least of valency two. Furthermore, multiple edges between a single pair of vertices are allowed if these edges are homotopically distinct (preserving planarity). After permuting over all distinct labels of the vertices, we partition the set of graphs into three groups (cf. Figure 6):

- (i) Graphs in which the operators $1, \dots, n$ are connected by simple edges, such that they form a polygon (i.e. an n -cycle),
- (ii) graphs in which at least one pair of adjacent operators $(i, i + 1)$ is not connected by a propagator, and
- (iii) graphs in which the operators $1, \dots, n$ form an n -cycle, and at least one pair of adjacent operators $(i, i + 1)$ is connected by two or more propagators.

We argue that only the first set of graphs (i) reveals a non-zero contribution after taking the 10d null polygonal limit of the generating function. Consider, the second set of graphs (ii). These graphs miss at least one edge on the perimeter of the polygon, and thus, do not obtain a

⁷See [36] for a detailed explanation on how to apply the twistor Feynman rules to obtain the loop integrands (also reviewed in Section 3 of [14]). These rules are applied in the same manner to the disk-topology graphs in $\Gamma_{n,\ell}^{\text{disk}}$.

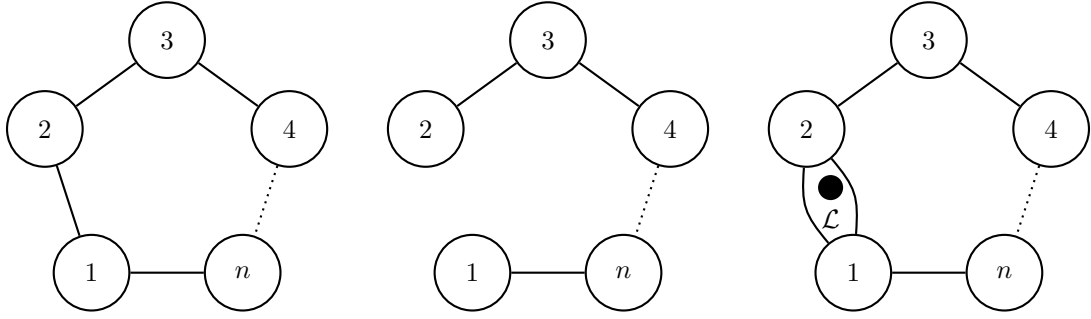


Figure 6: Depicted are exemplary graphs that contribute to an n -point generating function. In the first set of graphs on the left, adjacent external operators are connected by a simple fat propagator. Not depicted are the Lagrangians or propagators connecting them to each other or to external operators, or propagators connecting non-adjacent operators. In the second set of graphs, at least one pair of non-adjacent operators is not connected – here, the operators 1 and 2. And finally on the right, at least one propagator on the perimeter is split into two edges, which is only possible if they enclose at least one Lagrangian insertion.

factor $D_{i,i+1} = x_{i,i+1}^2 / X_{i,i+1}^2$ for at least one $i = 1, \dots, n$, after applying the twistor Feynman rules. Consequently, taking the residue (4.1) at $X_{i,i+1}^2 \rightarrow 0$ eliminates any contribution obtained from such graphs.

Summing up the third set of graphs (iii) will inherently lead to a zero contribution. Since all external operators form the boundary of the disk, two adjacent external operators can only be connected by two or more propagators if these propagators enclose Lagrangian insertions. This will effectively lead to an isolated loop integrand of a two-point function which is zero.

Now that we have restricted the graphs to group (i), we can reduce the set further by considering that the polygons are the square roots of the residues (2.12), (3.2). The square root has a natural interpretation in terms of these graphs. The external operators form a polygon that cuts the color surface into two regions with disk topology (an “inside” and an “outside”). Depending on whether the Lagrangian insertions are located on the inside or outside of the polygon, or split between the two regions, different contributions of products of polygon expressions are obtained. At two loops, for example, the residue can be written schematically as follows

$$R_{n,2} = \text{Graph 1} + \text{Graph 2} + 2 \times \text{Graph 3}. \quad (4.2)$$

where Graph 1, Graph 2, and Graph 3 are shown in Figure 6. Graph 1 has two Lagrangian insertions on the inside of the polygon. Graph 2 has two Lagrangian insertions on the outside of the polygon. Graph 3 has one Lagrangian insertion on the inside and one on the outside.

As can be seen from this equation, all Lagrangian insertions have to be gathered inside (or outside) of the polygon to obtain the relevant loop correction, while the propagators on the outside (or inside) will form the tree-level polygon result. Products of lower loop polygons are obtained if the Lagrangians are distributed in both regions. The polygon $M_{n,\ell}$ can thus

be isolated by restricting the graphs to disk topology with the perimeter being single edged propagators connecting adjacent operators.⁸

Hence, the polygons are obtained by applying the twistor Feynman rules to the graphs with disk topology $\Gamma_{n,\ell}^{\text{disk}}$ and taking the 10d null polygonal limit as formulated in (4.1).

By exactly the same reasoning, the factorization (2.13) of polygons into smaller polygons upon taking further ten-dimensional null limits directly follows.

Ansatz. We have found a way to compute the polygons directly from twistors, but the general drawback of the twistor formulation still applies: The result contains the (arbitrary but fixed) reference twistor. While the final expression is ultimately independent of this reference twistor, it is virtually impossible to remove the reference twistor from it to write it in terms of basic invariants (i. e. square distances). As usual, we therefore resort to writing a suitable manifestly invariant ansatz, and match it against the twistor result by numerical evaluation.

The ansatz has the general form

$$M_{n,\ell} = \sum_a f_a(x_{ij}^2, y_{ij}^2) \mathcal{I}_a(x_{ij}^2), \quad (4.3)$$

where the \mathcal{I}_a form a basis of rational functions that are the integrands of conformal integrals planarly embedded inside the polygon, and $f_a(x_{ij}^2, y_{ij}^2)$ are polynomial coefficient functions. An obstacle in the computation is that there appears to be no way to bound the coefficients f_a from first principles, so we have to partially resort to educated guesses to formulate ansätze that are both sufficiently general and not too big to constrain.

5 All 10d Null Polygons to Two Loops

Using the twistor Feynman rules on graphs with disk topology enables us to compute the polygons $M_{n,\ell}$ directly, without having to find the full n -point ℓ -loop generating function first. At one-loop order, the explicit expression of the square (3.6), the pentagon (3.12), and the hexagon (3.24) are sufficient to state a formula for all one-loop polygons that includes both the parity-even and parity-odd parts. We have verified this proposal numerically up to nine points by matching against the respective twistor expressions.

At two loops, we focus on the parity-even part of the polygons, by numerically matching appropriate ansätze against the twistor computation, as described above. In this way, we successively compute two-loop polygons starting from six points. We find systematics in their expressions that further constrain the ansatz for respective higher-point polygons. Reaching the ten-sided polygon, we could fix all patterns in the expression, and thus conjecture a formula for the parity-even part of all polygons $M_{n,2}$ at two loops. We checked that proposal explicitly at eleven points, and find agreement with the twistor result.

The final result for all polygons $M_{n,\ell}$ for any n and up to $\ell = 2$ loops is attached in the ancillary MATHEMATICA file `polygons.m`.

Before presenting the formulae for all one-loop and two-loop polygons in (5.1), (5.11), and (5.13) below, let us describe how the factorization property of the polygons can be used to organize them systematically.

⁸While the propagators naturally split between the inside and outside of the polygon, one might have to worry about the dressing factors of the vertices $V_{j_1 \dots j_k}^i$ when applying the Feynman rules. (Here, i denotes the respective vertex and the lower indices reflect the cyclic ordering of the edges around i .) Since the dressing factor can be written as a product of factors depending only on neighboring edges $V_{j_1 \dots j_k}^i = \Delta_{j_1 j_2}^i \dots \Delta_{j_k j_1}^i$ (see (3.33) in [36]), they also factorize along the perimeter of the polygon.

5.1 Factorization Channels

The polygon integrands are rational functions of ten-dimensional distances X_{ij}^2 as well as four-dimensional distances x_{ij}^2 (four-dimensional propagators $d_{i,j}$ appear only polynomially). In particular, they display ten-dimensional poles. Like all rational functions, they are fixed by the residues at their poles, and their behavior at infinity. The poles are precisely the factorization channels, on which the polygons factorize into products of lower polygons (2.15). After taking these residues into account, what remains are terms that are free of ten-dimensional propagators $D_{ij} = x_{ij}^2/X_{ij}^2$ on the diagonals of the polygon (the “empty” polygon).

The factorization property (2.15) as well as the above picture inspire the following natural decomposition of the polygons \mathbb{M}_n into more basic building blocks \mathbb{F}_f that we call *faces*:

$$\mathbb{M}_n = \mathbb{F}_{1,\dots,n} + \sum_{\substack{\Gamma \in \text{tree} \\ \text{graphs}}} \prod_{\substack{\text{edges} \\ (ij) \in \Gamma}} D_{ij} \times \prod_{\substack{\text{faces} \\ f \in \Gamma}} \mathbb{F}_f. \quad (5.1)$$

Here, the sum runs over all tree graphs that contribute to $M_{n,0}$, excluding the empty polygon graph (whose contribution is captured by the first term).⁹ The formula (5.1)

- defines the faces $\mathbb{F}_{1,\dots,n}$ recursively in terms of the polygons \mathbb{M}_n as well as the lower-point and lower-loop faces,
- makes the polygon factorization property (2.15) manifest,¹⁰
- and it reduces the polygon functions \mathbb{M}_n to yet simpler functions, the faces $\mathbb{F}_{1,\dots,n}$.

In order to apply (5.1) perturbatively, we expand both the polygons \mathbb{M}_n (cf. (2.11)) and the faces $\mathbb{F}_{1,\dots,n}$ in the coupling,

$$\mathbb{F}_{1,\dots,n} = 1 + \sum_{\ell=1}^{\infty} \frac{(-g^2)^\ell}{\ell!} \int \left[\prod_k \frac{d^4 x_k}{\pi^2} \right] F_{1,\dots,n}^{(\ell)}, \quad (5.2)$$

where the product over k is taken over all ℓ loop variables. We wrote the decomposition (5.1) in terms of the integrated objects \mathbb{M}_n and $\mathbb{F}_{1,\dots,n}$, but we emphasize that they hold at the level of the *integrands*, i. e. the integrations can be removed from the equation. At integrand level, one must symmetrize each term over all distributions of integration points (Lagrangian insertions) on the factors F_f , exactly as it happens in (2.10) and (2.13).

Notably, the leading order $F_{1,\dots,n}^{(0)}$ of the faces are trivial by construction, and the triangles receive no loop corrections:

$$\mathbb{F}_{i_1,i_2,i_3} = 1. \quad (5.3)$$

Let us exemplify the decomposition (5.1) by explicitly writing the expressions for the square, pentagon and hexagon. The former two are expressed as

$$\mathbb{M}_4 = \mathbb{F}_{1,2,3,4} + D_{13} \times \mathbb{F}_{1,2,3} \mathbb{F}_{1,3,4} + D_{24} \times \mathbb{F}_{1,2,4} \mathbb{F}_{2,3,4}, \quad (5.4)$$

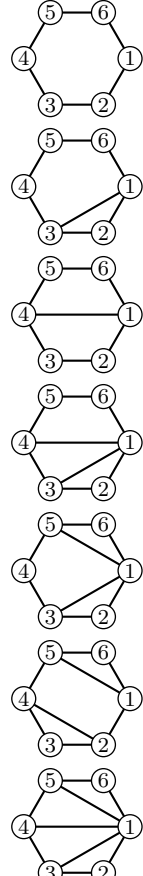
$$\mathbb{M}_5 = \mathbb{F}_{1,2,3,4,5} + \left[\frac{1}{2} D_{14} \times \mathbb{F}_{1,2,3,4} \mathbb{F}_{1,4,5} + \frac{1}{2} D_{14} D_{13} \times \mathbb{F}_{1,2,3} \mathbb{F}_{1,3,4} \mathbb{F}_{1,4,5} + (\text{D}_5 \text{ perms}) \right], \quad (5.5)$$

⁹These graphs are exactly the planar graphs one can draw on the disk with n punctures on the boundary (and no internal vertices), i. e. all graphs that tessellate the n -gon by diagonals. See the first line of Table 1, as well as [56] for their counting modulo dihedral permutations.

¹⁰Starting with the factorization property of the polygons \mathbb{M}_n , there is some freedom in the definition of the faces \mathbb{F} , in the sense that one could write variations of the formula (5.1), that would differ by re-arrangements of the geometric series in the fat propagators, e.g. $D_{ij}/d_{ij} = 1 + D_{ij}$. We find that our choice (5.1) yields the most natural definition.

while the hexagon is split into tree-level faces as follows:

$$\begin{aligned}
\mathbb{M}_6 &= \mathbb{F}_{1,2,3,4,5,6} \\
&+ \left[\frac{1}{2} D_{13} \times \mathbb{F}_{1,2,3} \mathbb{F}_{3,4,5,6,1} \right. \\
&\quad + \frac{1}{4} D_{14} \times \mathbb{F}_{1,2,3,4} \mathbb{F}_{4,5,6,1} \\
&\quad + D_{13} D_{14} \times \mathbb{F}_{1,2,3} \mathbb{F}_{3,4,1} \mathbb{F}_{4,5,6,1} \\
&\quad + \frac{1}{2} D_{13} D_{15} \times \mathbb{F}_{1,2,3} \mathbb{F}_{5,6,1} \mathbb{F}_{3,4,5,1} \\
&\quad + \frac{1}{4} D_{15} D_{24} \times \mathbb{F}_{2,3,4} \mathbb{F}_{5,6,1} \mathbb{F}_{1,2,4,5} \\
&\quad + \frac{1}{2} D_{13} D_{14} D_{15} \times \mathbb{F}_{1,2,3} \mathbb{F}_{1,3,4} \mathbb{F}_{1,4,5} \mathbb{F}_{1,5,6} + \dots \\
&\quad \left. + (\text{D}_6 \text{ perms}) \right], \tag{5.6}
\end{aligned}$$



where the dots stand for two more terms that are products of three propagators D_{ij} and four triangle faces $\mathbb{F}_{i_1, i_2, i_3}$. Expanding these expressions at one-loop order using (5.2), and passing to the integrands yields

$$M_{4,1} = F_{1,2,3,4}^{(1)}, \tag{5.7}$$

$$M_{5,1} = F_{1,2,3,4,5}^{(1)} + \left[\frac{1}{2} D_{14} \times F_{1,2,3,4}^{(1)} + (\text{D}_5 \text{ perms}) \right], \tag{5.8}$$

$$\begin{aligned}
M_{6,1} &= F_{1,2,3,4,5,6}^{(1)} + \left[\frac{1}{2} D_{13} \times F_{3,4,5,6,1}^{(1)} + \frac{1}{4} D_{14} \times (F_{1,2,3,4}^{(1)} + F_{4,5,6,1}^{(1)}) + D_{13} D_{14} \times F_{4,5,6,1}^{(1)} \right. \\
&\quad \left. + \frac{1}{2} D_{13} D_{15} \times F_{3,4,5,1}^{(1)} + \frac{1}{4} D_{15} D_{24} \times F_{1,2,4,5}^{(1)} + (\text{D}_6 \text{ perms}) \right]. \tag{5.9}
\end{aligned}$$

At two-loop order, these expressions almost stay the same, up to the substitution $F^{(1)} \rightarrow F^{(2)}$. Only the two-loop hexagon receives an extra term that is a product of two one-loop squares (from the third line of (5.6)):

$$M_{6,2} = (5.9) \Big|_{F^{(1)} \rightarrow F^{(2)}} + \left[\frac{1}{2} D_{14} \times F_{1,2,3,4}^{(1)} F_{1,4,5,6}^{(1)} + (\text{D}_6 \text{ perms}) \right]. \tag{5.10}$$

Importantly, terms of this type can contain products of parity-odd terms that contribute to the parity-even part of $M_{n,2}$. The four-point faces $F_{1,2,3,4}^{(\ell)}$ are free of parity-odd parts, but $F_{i_1, \dots, i_n \geq 5}^{(1)}$ does contain parity-odd terms, and thus starting from $M_{8,2}$, products of such terms do contribute to the decomposition (5.1). This highlights that it is important to include

both parity-even and parity-odd parts in the definition of the polygons M_n and the faces $F_{1,\dots,n}$ in order to make the decomposition (5.1) consistent. The same happens for massless amplitudes, where parity-odd terms have to be included in order to consistently establish the super-correlator/super-amplitude duality [47, 48].

5.2 One-Loop Result

The expressions for the square (3.6), the pentagon (3.12), and the hexagon (3.24) suffice to conjecture the general structure of both the even and odd part of all one-loop polygons. The corresponding one-loop faces that dress the tree-level graphs for any $n \geq 4$ are

$$F_{i_1, i_2, \dots, i_n}^{(1)} = \sum_{\substack{[i_m, i_{m+1}], [i_l, i_{l+1}] \\ \text{non-adjacent}}} \frac{P_{i_m i_{l+1}, i_{m+1} i_l} - 4i \epsilon_{\mu\nu\rho\sigma} x_{i_m 0}^\mu x_{i_{m+1} 0}^\nu x_{i_l 0}^\rho x_{i_{l+1} 0}^\sigma}{2 x_{i_m 0}^2 x_{i_{m+1} 0}^2 x_{i_l 0}^2 x_{i_{l+1} 0}^2} - \sum_{1 \leq j < k < l < m \leq n} \frac{y_{i_j i_l}^2 y_{i_k i_m}^2}{x_{i_j 0}^2 x_{i_k 0}^2 x_{i_l 0}^2 x_{i_m 0}^2}, \quad (5.11)$$

where the first sum runs over all pairs of non-adjacent edges at the perimeter of the polygon. The imaginary term proportional to $\epsilon_{\mu\nu\rho\sigma}$ is parity-odd, all other terms are parity-even, x_0 is the coordinate of the Lagrangian insertion, and we defined the combination

$$P_{ij,kl} = -x_{ij}^2 x_{kl}^2 + x_{ik}^2 x_{jl}^2 + x_{il}^2 x_{jk}^2. \quad (5.12)$$

We have verified this proposal by numerically comparing it to the respective twistor expressions (4.1) up to nine points.

5.3 Two-Loop Result

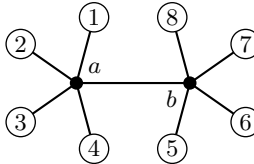
The formula for the two-loop faces $F_{1,\dots,n}^{(2)}$ is more intricate, and we only computed its parity-even part. Hence also the two-loop polygons M_n are restricted to their parity-even parts. We will not indicate the superscript ‘‘even’’, with the understanding that all two-loop expressions refer to their parity-even parts only.

Result. We decompose the two-loop n -point faces in exactly the same way as was done for the integrand of the two-loop n -point massless gluon amplitude [57]:¹¹

$$F_{1,\dots,n}^{(2)} = \sum_{k,\mathbf{e}} f_{k,\mathbf{e},a,b}(x_{ij}^2, y_{ij}^2) \mathcal{J}_k^{e,a,b} + (a \leftrightarrow b). \quad (5.13)$$

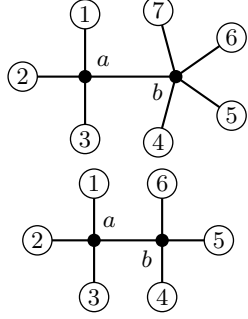
Here, the sum over k runs over three different propagator topologies $\mathcal{J}_k^{e,a,b}$, the sum over \mathbf{e} runs over their planar embeddings in the face $F_{1,\dots,n}$, and the coefficients $f_{k,\mathbf{e},a,b}$ are polynomials in the basic scalar invariants x_{ij}^2 and y_{ij}^2 .

The following three propagator topologies occur in the decomposition:



$$\mathcal{J}_1^{1,\dots,8,a,b} = \frac{1}{x_{1a}^2 x_{2a}^2 x_{3a}^2 x_{4a}^2 x_{ab}^2 x_{5b}^2 x_{6b}^2 x_{7b}^2 x_{8b}^2}, \quad (5.14)$$

¹¹The two-loop faces (5.13) as well as the resulting two-loop polygons (5.1) are constructed in the ancillary MATHEMATICA file `polygons.m`. The coefficients $f_{k,\mathbf{e},a,b}$ are stored in the file `twoLoopCoefficients.m`.



$$\mathcal{J}_2^{1,\dots,7,a,b} = \frac{1}{x_{1a}^2 x_{2a}^2 x_{3a}^2 x_{ab}^2 x_{4b}^2 x_{5b}^2 x_{6b}^2 x_{7b}^2}, \quad (5.15)$$

$$\mathcal{J}_3^{1,\dots,6,a,b} = \frac{1}{x_{1a}^2 x_{2a}^2 x_{3a}^2 x_{ab}^2 x_{4b}^2 x_{5b}^2 x_{6b}^2}. \quad (5.16)$$

Note that the structures \mathcal{J}_1 , \mathcal{J}_2 , \mathcal{J}_3 do not include numerator factors, which means that they do not absorb all dependence on the Lagrangian points a , b .¹² Therefore, the coefficients $f_{k,e,a,b}$ must not only contain factors x_{ij}^2 between external points $i, j \leq n$, but also among external points $i \leq n$ and Lagrangian points $j \in \{a, b\}$. However, they may not contain factors that cancel any of the denominator factors in the definitions of the integrands \mathcal{J}_1 , \mathcal{J}_2 , \mathcal{J}_3 . The only exception to this is the coefficient $f_{1,e,a,b}$ of the double-penta integrand, which may include terms with a factor x_{ab}^2 that turns \mathcal{J}_1 into the product of two one-loop box integrands.

The sum over \mathbf{e} runs over all planar embeddings of the integrands \mathcal{J}_1 , \mathcal{J}_2 , \mathcal{J}_3 into the polygonal face $F_{1,\dots,n}$. For example, the double-penta integrand \mathcal{J}_3^e is summed over embeddings

$$\mathbf{e} = (i_1, \dots, i_8), \quad i_1 < i_2 < i_3 < i_4 \leq i_5 < i_6 < i_7 < i_8 \leq i_1 \pmod{n}. \quad (5.17)$$

Making use of the dihedral D_n symmetry, we can fix $i_1 = 1$. Due to the planar embedding, we can equally sum over the distances ℓ_k of neighboring points that attach to the integrand:

$$\tilde{\mathbf{e}} = [\ell_1, \dots, \ell_8], \quad \ell_k = i_k - i_{k-1} \quad (i_0 \equiv i_8), \quad \ell_k \geq \begin{cases} 1 & k = 2, 3, 4, 6, 7, 8, \\ 0 & k = 1, 5. \end{cases} \quad (5.18)$$

We use round/square brackets to distinguish the two notations. The coefficient functions $f_{k,e,a,b}$ are polynomials in x_{ij}^2 , $i, j \in \{1, \dots, n, a, b\}$, and y_{ij}^2 , $i, j \in \{1, \dots, n\}$. For $y_{ij}^2 = 0$, they reduce to the coefficients of the massless gluon amplitude integrand (2.16), which was determined in [57].¹³ The coefficient $f_{1,e,a,b}$ of the double-penta integrand \mathcal{J}_1 can be written in a relatively compact way:¹⁴

$$4 f_{1,i_1,\dots,i_8,a,b} = x_{ab}^2 \left(\delta_{\ell_2,1} \delta_{\ell_4,1} P_{i_1 i_4, i_2 i_3} - 2 y_{i_1 i_3}^2 y_{i_2 i_4}^2 \right) \left(\delta_{\ell_6,1} \delta_{\ell_8,1} P_{i_5 i_8, i_6 i_7} - 2 y_{i_5 i_7}^2 y_{i_6 i_8}^2 \right) \\ - \delta_{\ell_2,1} \delta_{\ell_4,1} \delta_{\ell_6,1} \delta_{\ell_8,1} \begin{bmatrix} i_1 & i_2 & i_3 & i_4 & a \\ i_5 & i_6 & i_7 & i_8 & b \end{bmatrix} + \delta_{\ell_1,0} \delta_{\ell_3,1} \delta_{\ell_5,0} \delta_{\ell_7,1} y_{i_1 i_4}^2 h_{\text{DP}}, \quad (5.19)$$

with the factor h_{DP} given by

$$h_{\text{DP}} = \begin{bmatrix} i_1 & i_2 & i_3 & a \\ i_4 & i_6 & i_7 & b \end{bmatrix} + \begin{bmatrix} i_2 & i_3 & i_4 & a \\ i_6 & i_7 & i_1 & b \end{bmatrix} - x_{i_1 i_4}^2 \begin{bmatrix} i_2 & i_3 & a \\ i_6 & i_7 & b \end{bmatrix} \\ - x_{ab}^2 \left(x_{i_2 i_3}^2 P_{i_1 i_7, i_4 i_6} + x_{i_6 i_7}^2 P_{i_1 i_2, i_3 i_4} - x_{i_1 i_4}^2 x_{i_2 i_3}^2 x_{i_6 i_7}^2 \right), \quad (5.20)$$

¹²See Appendix A for an equivalent decomposition in terms of integrands of conformal integrals that include the numerator factors.

¹³Setting $y_{i,j}^2 = 0$ for all i, j in particular includes passing to the four-dimensional null limit $x_{i,i+1}^2 = 0$ at the perimeter of the polygon, due to the ten-dimensional null condition $0 = X_{i,i+1}^2 = x_{i,i+1}^2 + y_{i,i+1}^2$.

¹⁴For compactness, we use both the i_k and the ℓ_k labels in this formula.

and where the square brackets denote determinants:

$$\begin{bmatrix} i_1 & i_2 & \dots \\ j_1 & j_2 & \dots \end{bmatrix} = \det \{x_{ij}^2\}_{\substack{i=i_1, i_2, \dots \\ j=j_1, j_2, \dots}}. \quad (5.21)$$

The numerator functions $f_{k,e}$ encode all two-loop faces $F_{1,\dots,n}^{(2)}$, and thereby all two-loop polygons $M_{n,2}$. Through the dependence on the embedding e , one could imagine that the number of functions $f_{k,e}$ proliferates as n increases. However, we see in the example of f_1 (5.19) that the dependence on the embedding is relatively moderate, in the sense that the expression stabilizes once all ℓ_j are sufficiently large. We observe that the same saturation property also holds for the other coefficients: In general, the coefficients cease to depend on the distances ℓ_j once $\ell_j \geq 2$:¹⁵

$$f_{k,[\dots, \ell_j, \dots]} = f_{k,[\dots, 2, \dots]} \quad \text{for } \ell_j \geq 2. \quad (5.22)$$

The only exception to this pattern are the distances $\ell_1 = i_1 - i_6$ and $\ell_4 = i_4 - i_3$ of the coefficients $f_{3,\hat{e}}$, where this saturation only occurs at $\ell_{1,4} \geq 3$. This is also the case for the integrand of the massless gluon amplitude [57]. Furthermore, the coefficient functions display the following label symmetries that are inherited from the symmetries of the respective propagator topologies \mathcal{J}_1 , \mathcal{J}_2 and \mathcal{J}_3 :

$$\begin{aligned} & f_{1,[\ell_1, \ell_2, \ell_3, \ell_4, \ell_5, \ell_6, \ell_7, \ell_8], a, b} & f_{2,[\ell_1, \ell_2, \ell_3, \ell_4, \ell_5, \ell_6, \ell_7], a, b} & f_{3,[\ell_1, \ell_2, \ell_3, \ell_4, \ell_5, \ell_6], a, b} \\ &= f_{1,[\ell_1, \ell_8, \ell_7, \ell_6, \ell_5, \ell_4, \ell_3, \ell_2], b, a} &= f_{2,[\ell_4, \ell_3, \ell_2, \ell_1, \ell_7, \ell_6, \ell_5], a, b} &= f_{3,[\ell_1, \ell_6, \ell_5, \ell_4, \ell_3, \ell_2], b, a} \\ &= f_{1,[\ell_5, \ell_6, \ell_7, \ell_8, \ell_1, \ell_2, \ell_3, \ell_4], b, a} & &= f_{3,[\ell_4, \ell_5, \ell_6, \ell_1, \ell_2, \ell_3], b, a} \\ &= f_{1,[\ell_5, \ell_4, \ell_3, \ell_2, \ell_1, \ell_8, \ell_7, \ell_6], a, b}, & &= f_{3,[\ell_4, \ell_3, \ell_2, \ell_1, \ell_6, \ell_5], a, b}. \end{aligned} \quad (5.23)$$

Assuming the saturation property as well as the label symmetries, we can list all potentially different coefficient functions $f_{k,e}$. In this way, we find that there are a priori 180 different coefficients $f_{1,\hat{e}}$, 156 different coefficients $f_{2,\hat{e}}$, and 88 different coefficients $f_{3,\hat{e}}$ corresponding to the three propagator topologies.

As seen above, the coefficients $f_{1,e}$ of the double-penta topology combine elegantly into (5.19). In contrast, the other two families $f_{2,e}$ and $f_{3,e}$ exhibit a considerably more intricate structure, with a subtler dependence on the embeddings. Their explicit forms can be found in the ancillary file `twoLoopCoefficients.m`.

Two-Loop Ansatz Construction. Having laid out the structure of the result, we now step back to outline how it was obtained. In order to match the twistor expression of the polygons to a manifestly Lorentz-invariant representation, it is necessary to formulate a compact ansatz. This ansatz is provided by the functions $f_{k,e}$, but with a priori undetermined numerical coefficients. Combining these functions with the denominators in (5.13), and using the factorization decomposition (5.1) yields an ansatz for the respective two-loop polygon.

Due to conformal symmetry, the coefficients $f_{k,a}$ are polynomials in x_{ij}^2 and d_{ij} , constructed such that each term becomes conformally invariant in x_{ij}^2 when combined with the

¹⁵In a strict sense, the saturation means the following: Given two planar embeddings $e = (i_1, \dots, i_j, i_{j+1}, \dots, i_{n_k})$ and $\hat{e} = (i_1, \dots, i_j, i_{j+1} + 1, \dots, i_{n_k} + 1)$ that only differ by increasing the distance between a single pair of indices by one, then

$$f_{k,\hat{e},a,b}|_{\hat{e} \rightarrow e} = f_{k,e,a,b} \quad \text{if } i_{j+1} - i_j \geq 2.$$

corresponding denominator \mathcal{J}_k .¹⁶ This property is directly inherited from the generating function $G_{n,\ell}$, which is itself conformal in the variables x_{ij}^2 when expressed as a function of d_{ij} and x_{ij}^2 . Consequently, this symmetry constrains the possible monomials in x_{ij}^2 that can appear in the polynomials $f_{k,a}$. Heuristically, we also observe that the appearance of the factors d_{ij} is similarly restricted: Each factor d_{ij} must be accompanied by a corresponding factor x_{ij}^2 , ensuring that $f_{k,a}$ remains a polynomial in the combined variables $(x_{ij}^2, y_{ij}^2 = x_{ij}^2 d_{ij})$. In other words, the functions $f_{k,e}$ are polynomials in x_{ij}^2 and y_{ij}^2 such that the conformal and R -charge weights of the products $f_{k,e} \mathcal{J}_k^e$ match those of the polygon correlator:

$$f_{k,e,a,b}(\lambda_i \lambda_j x_{ij}^2, \lambda_i \lambda_j y_{ij}^2) \mathcal{J}_k^{e,a,b}(\lambda_i \lambda_j x_{ij}^2) = \frac{f_{k,e,a,b}(x_{ij}^2, y_{ij}^2) \mathcal{J}_k^{e,a,b}(x_{ij}^2)}{\lambda_a^4 \lambda_b^4}. \quad (5.24)$$

Moreover, the functions $f_{k,e}$ do not contain distances x_{ij}^2 that cancel factors in the denominator of \mathcal{J}_k^e , with the exception of $f_{1,e}$, that may contain factors x_{ab}^2 , as was already mentioned above. Finally, the functions $f_{k,e}$ must obey the label symmetries (5.23), which further restricts the size of the ansätze. In this way, we find the number of unknown coefficients to be 1242, 240, and 50 for the functions $f_{1,e}$, $f_{2,e}$, and $f_{3,e}$, respectively (for fixed embeddings e). However, when inserting the ansätze into a specific face function F in an n -sided polygon $M_{n,2}$, the number of coefficients typically reduces, for three reasons: First, factors y_{ij}^2 are identified with x_{ij}^2 for $j = i + 1$. Second, part of the ansatz collapses if points in the embedding e are equal to another. Third, there might be identifications in the ansatz due to the dihedral symmetry D_n of the respective polygon.

The functions $f_{k,e}$ can now be probed in order of their appearance, beginning from the square $M_{4,2}$, and successively increasing the size of the polygons by one. At each step, the coefficients in the polynomials $f_{k,e}$ are fixed by comparison to the twistor expression, and subsequently fed into the succeeding ansatz. In this process, we can make use of the saturation property (5.22). To probe all degrees of freedom of the coefficient functions f_k , we would in principle have to push this process all the way to the two-loop hexadecagon $M_{16,2}$, such that all distances ℓ_j become saturated according to (5.22). However, the pattern of the various embeddings often becomes apparent much earlier. This is most notable for the double-penta functions $f_{1,e}$, which neatly combine into (5.19). In practice, we find the complete forms of all functions $f_{k,e}$ by matching the respective ansätze to polygons $M_{n,2}$ up to the decagon with $n = 10$. This yields a complete formula for all two-loop polygons. We have checked the resulting formula for the hendecagon $M_{11,2}$ by matching against the twistor computation, and found complete agreement. This verifies the correctness of the result for general n beyond reasonable doubt.

Examples: Square, Pentagon, and Hexagon. To exemplify the decomposition into different propagator topologies (5.1), we explicitly apply this formula up to six points. For the square and pentagon, the two-loop faces read:

$$F_{1,2,3,4}^{(2)} = \frac{1}{4} f_{3,[0,1,1,0,1,1]} \mathcal{J}_3^e + (\text{D}_4 \text{ perms}), \quad (5.25)$$

$$F_{1,2,3,4,5}^{(2)} = f_{3,[0,1,1,0,1,2]} \mathcal{J}_3^e + \frac{1}{2} f_{3,[0,1,1,1,1,1]} \mathcal{J}_3^e + \frac{1}{2} f_{2,[0,1,1,0,1,1,1]} \mathcal{J}_2^e + (\text{D}_5 \text{ perms}), \quad (5.26)$$

with the coefficient functions given by

$$f_{3,[0,1,1,0,1,1]} = (x_{13}^2 - y_{13}^2) (x_{13}^2 x_{24}^2 - y_{13}^2 y_{24}^2),$$

¹⁶The terms become conformally invariant after integration, so the integrands are of conformal weight zero in the external points and of weight 4 in the integration variables a and b .

$$\begin{aligned}
f_{3,[0,1,1,0,1,2]} &= \frac{1}{2}(x_{13}^2 - y_{13}^2) \left(P_{15,23} - 2y_{13}^2 y_{24}^2 \right), \\
f_{3,[0,1,1,1,1,1]} &= -\frac{1}{2}P_{12,45} x_{13}^2 + \frac{1}{2}P_{12,35} (x_{14}^2 - y_{14}^2) - \frac{1}{2}y_{13}^2 \left(P_{15,24} - 2y_{14}^2 y_{25}^2 \right), \\
f_{2,[0,1,1,0,1,1,1]} &= \frac{1}{2}x_{2b}^2 \left(P_{16,35} y_{13}^2 + x_{13}^2 \left(P_{13,56} - 2y_{14}^2 y_{35}^2 \right) \right), \tag{5.27}
\end{aligned}$$

where $P_{ij,kl}$ is defined in (5.12). In the above equations, the coefficients $f_{k,\bar{e}}$ are labeled by the distances ℓ_j between neighboring points in the embedding, as in (5.18). It is implied that the corresponding point labels start with point one, that is $\mathbf{e} = (1, 1 + \ell_2, \dots)$, and that the respective factors \mathcal{J}_k^e are defined with this embedding \mathbf{e} .

According to (5.7), the two-loop square $M_{4,2}$ equals the two-loop four-point face, and (5.25) consistently matches the expression (3.7) for $M_{4,2}$ obtained from the generating function. In order to obtain the two-loop pentagon $M_{5,2}$, the five-point face (5.26) must be combined with the four-point face as in (5.8). Once more, the expression (3.13) derived from the generating function is correctly reproduced.

The six-point face at two-loop order already consists of a much larger number of propagator topologies:

$$\begin{aligned}
F_{1,2,3,4,5,6}^{(2)} &= f_{3,[0,1,1,0,1,3]} \mathcal{J}_3^e + \frac{1}{2}f_{3,[0,1,1,0,2,2]} \mathcal{J}_3^e + f_{3,[0,1,1,1,1,2]} \mathcal{J}_3^e + f_{3,[0,1,1,1,2,1]} \mathcal{J}_3^e \\
&\quad + \frac{1}{2}f_{3,[0,1,1,2,1,1]} \mathcal{J}_3^e + \frac{1}{2}f_{3,[0,1,2,0,1,2]} \mathcal{J}_3^e + \frac{1}{2}f_{3,[0,1,2,0,2,1]} \mathcal{J}_3^e + \frac{1}{4}f_{3,[1,1,1,1,1,1]} \mathcal{J}_3^e \\
&\quad + f_{2,[0,1,1,0,1,1,2]} \mathcal{J}_2^e + \frac{1}{2}f_{2,[0,1,1,0,1,2,1]} \mathcal{J}_2^e + f_{2,[0,1,1,1,1,1,1]} \mathcal{J}_2^e + f_{2,[0,1,2,0,1,1,1]} \mathcal{J}_2^e \\
&\quad + \frac{1}{4}f_{1,[0,1,1,1,0,1,1,1]} \mathcal{J}_1^e + (\text{D}_6 \text{ perms}). \tag{5.28}
\end{aligned}$$

In particular, the double-penta topology \mathcal{J}_1 appears for the first time. Again, the coefficients are labeled by to the distances between neighboring points, and are given by

$$\begin{aligned}
f_{3,[0,1,1,0,1,3]} &= \frac{1}{2}(x_{13}^2 - y_{13}^2) \left(P_{15,23} - 2y_{13}^2 y_{24}^2 \right), \\
f_{3,[0,1,1,0,2,2]} &= -y_{13}^2 y_{25}^2 (x_{13}^2 + y_{13}^2), \\
f_{3,[0,1,1,1,1,2]} &= -\frac{1}{2}x_{15}^2 (x_{13}^2 x_{24}^2 - y_{13}^2 y_{24}^2) + \frac{1}{4}P_{12,35} (x_{14}^2 - y_{14}^2) + \frac{1}{2}y_{13}^2 (2y_{14}^2 y_{25}^2 - P_{15,24}), \\
f_{3,[0,1,1,1,2,1]} &= -\frac{1}{4}P_{15,23} x_{14}^2 + \frac{1}{2}x_{12}^2 x_{13}^2 x_{46}^2 - \frac{1}{2}x_{16}^2 y_{13}^2 y_{24}^2 - \frac{1}{4}y_{14}^2 (P_{12,35} - 4y_{13}^2 y_{26}^2), \\
f_{3,[0,1,1,2,1,1]} &= -\frac{1}{2}P_{15,24} y_{13}^2 - \frac{1}{2}y_{15}^2 (P_{12,35} - 2y_{13}^2 y_{26}^2), \\
f_{3,[0,1,2,0,1,2]} &= \frac{1}{2}(x_{14}^2 - y_{14}^2) \left(\frac{1}{2}P_{15,23} + x_{12}^2 x_{45}^2 - 2y_{14}^2 y_{25}^2 \right), \\
f_{3,[0,1,2,0,2,1]} &= \frac{1}{4}(x_{14}^2 - y_{14}^2) (P_{15,23} - 2x_{12}^2 x_{46}^2 - 4y_{14}^2 y_{26}^2), \\
f_{3,[1,1,1,1,1,1]} &= \frac{1}{4} \left(\begin{bmatrix} 2 & 3 & 4 \\ 5 & 6 & 1 \end{bmatrix} + \begin{bmatrix} 6 & 1 & 2 \\ 3 & 4 & 5 \end{bmatrix} + P_{25,46} x_{13}^2 + P_{13,25} x_{46}^2 + P_{25,36} y_{14}^2 + P_{14,25} y_{36}^2 \right. \\
&\quad \left. - 2x_{56}^2 y_{13}^2 y_{24}^2 - 2x_{45}^2 y_{13}^2 y_{26}^2 - 2x_{23}^2 y_{15}^2 y_{46}^2 - 2x_{12}^2 y_{35}^2 y_{46}^2 + 4y_{13}^2 y_{25}^2 y_{46}^2 \right), \\
f_{2,[0,1,1,0,1,1,2]} &= \frac{1}{2}x_{2b}^2 \left(P_{16,35} y_{13}^2 - 2x_{13}^2 y_{14}^2 y_{35}^2 \right), \\
f_{2,[0,1,1,0,1,2,1]} &= \frac{1}{2}x_{13}^2 x_{2b}^2 \left(P_{13,56} - 2y_{14}^2 y_{36}^2 \right),
\end{aligned}$$

$$\begin{aligned}
f_{2,[0,1,1,1,1,1,1]} &= \frac{1}{4} \left(- \begin{bmatrix} 1 & 2 & 3 & 4 \\ 5 & 6 & 1 & b \end{bmatrix} - \begin{bmatrix} 1 & 2 & 3 \\ 5 & 6 & b \end{bmatrix} y_{14}^2 \right. \\
&\quad \left. + (x_{13}^2 x_{2b}^2 - x_{12}^2 x_{3b}^2) (P_{14,56} + x_{56}^2 y_{14}^2 - 2y_{15}^2 y_{46}^2) \right), \\
f_{2,[0,1,2,0,1,1,1]} &= \frac{1}{4} x_{2b}^2 (P_{16,35} y_{14}^2 + x_{14}^2 (P_{13,56} - 2y_{15}^2 y_{46}^2)), \\
f_{1,[0,1,1,1,0,1,1,1]} &= \frac{1}{4} x_{ab}^2 (P_{14,23} - 2y_{13}^2 y_{24}^2) (P_{14,56} - 2y_{15}^2 y_{46}^2) - \frac{1}{4} \begin{bmatrix} 1 & 2 & 3 & 4 & a \\ 4 & 5 & 6 & 1 & b \end{bmatrix} + \frac{1}{4} y_{14}^2 h_{\text{DP}},
\end{aligned} \tag{5.29}$$

where again it is understood that $e = (1, 1 + \ell_2, \dots)$ starts with the point label 1. The last (double-penta) coefficient $f_{1,\dots}$ can be obtained from (5.19), with the factor h_{DP} given in (5.20). In accordance with the saturation property (5.22), one can see that $f_{3,[0,1,1,0,1,3]} = f_{3,[0,1,1,0,1,2]}$. The two-loop hexagon $M_{6,2}$ can then be obtained by using (5.10), and plugging in the expressions for the two-loop four-point and five-point faces as well as the product of one-loop squares.

6 Interacting 10d Null Polygons

We obtain the interacting polygonal correlator \mathbb{M}_n (2.11) by integrating over the positions $x_{n+1}, \dots, x_{n+\ell}$ of the Lagrangian insertions that appear in the integrands $M_{n,\ell}$ discussed so far. Explicitly, up to two loops we have

$$\mathbb{M}_n = M_{n,0} - \frac{1}{2} g^2 \int \frac{d^4 x_{n+1}}{\pi^2} M_{n,1} + \frac{1}{2} g^4 \iint \frac{d^4 x_{n+1}}{\pi^2} \frac{d^4 x_{n+2}}{\pi^2} M_{n,2} + \mathcal{O}(g^6). \tag{6.1}$$

In the following, we analyze the interacting polygon correlators, focusing on the particular case of the pentagon at one and two loops.

6.1 Pentagon at Integrated Level

Very little is known about the integrated pentagon in perturbation theory. At two loops, the (completely off-shell) five-point conformal integrals \mathcal{I}_6 and \mathcal{I}_7 (3.15) are not known for general space-time configurations. But they have been computed in some physically relevant kinematical limits [13], which we address below. Collecting (3.12) and (3.13), the two-loop pentagon can be written as

$$\begin{aligned}
\mathbb{M}_5 &= \frac{1}{5} M_{5,0} - \frac{g^2}{2} p_{1234} \mathbb{I}_1^{[1234]} + \frac{g^4}{2} p_{1234} x_{14}^2 (1 - d_{14}) \mathbb{I}_6^{[14|23|5]} \\
&\quad + \frac{g^4}{2} p_{1234} (x_{13}^2 (1 - d_{13}) \mathbb{I}_5^{[13|24]} + x_{24}^2 (1 - d_{24}) \mathbb{I}_5^{[24|13]}) \\
&\quad + \frac{g^4}{2} (x_{35}^2 (1 - d_{35}) q_{12345} + x_{13}^2 (1 - d_{13}) q_{54321}) \mathbb{I}_7^{[12|45|3]} + (\text{C}_5 \text{ perms}) + \mathcal{O}(g^6),
\end{aligned} \tag{6.2}$$

where $+(\text{C}_5 \text{ perms})$ stands for summing over cyclic permutations, the factor $1/5$ compensates for over-counting the tree-level contribution, and the factors p and q are defined in (3.16), (3.17). The conformal integrals appearing above follow from the respective integrands (3.8), (3.9), and (3.15), and are given by

$$\mathbb{I}_1^{[1234]} = \int \frac{d^4 x_6}{\pi^2} \frac{1}{x_{16}^2 x_{26}^2 x_{36}^2 x_{46}^2} = \frac{F_1(z_1, \bar{z}_1)}{x_{13}^2 x_{24}^2}, \tag{6.3}$$

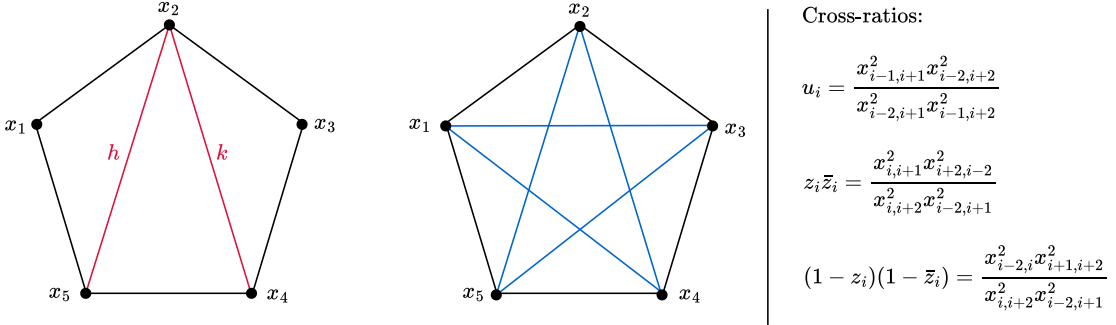


Figure 7: The two type of pentagon configuration we consider: on the first the point x_2 has h and k bridges to the points x_5 and x_4 , respectively. On the second, we will argue that even when all highlighted bridges are non-zero the pentagon is still planar and non-trivial. On the right, the cross-ratios we use to parametrize this five point correlation function.

$$\mathbb{I}_5^{[12|34]} = \iint \frac{d^4 x_6}{\pi^2} \frac{d^4 x_7}{\pi^2} \frac{1}{(x_{16}^2 x_{26}^2 x_{36}^2) x_{67}^2 (x_{17}^2 x_{27}^2 x_{47}^2)} = \frac{F_2\left(\frac{1}{z_1}, \frac{1}{\bar{z}_1}\right)}{x_{12}^2 x_{34}^2}, \quad (6.4)$$

$$\mathbb{I}_6^{[12|34|5]} = \iint \frac{d^4 x_6}{\pi^2} \frac{d^4 x_7}{\pi^2} \frac{x_{56}^2}{(x_{16}^2 x_{26}^2 x_{36}^2 x_{46}^2) x_{67}^2 (x_{17}^2 x_{27}^2 x_{57}^2)}, \quad (6.5)$$

$$\mathbb{I}_7^{[12|34|5]} = \iint \frac{d^4 x_6}{\pi^2} \frac{d^4 x_7}{\pi^2} \frac{1}{(x_{36}^2 x_{46}^2 x_{56}^2) x_{67}^2 (x_{17}^2 x_{27}^2 x_{57}^2)}. \quad (6.6)$$

Due to conformal symmetry, five-point correlators and the integrals (6.3)–(6.6) are functions of five independent conformal cross-ratios u_i , which we define in Figure 7. There, we also introduce an over-complete ten-element set of cross-ratios z_i, \bar{z}_i , $i = 1, \dots, 5$, which will be useful to write the four-point sub-correlators of the polygons (and four-point integrals) which depend on just a pair of cross-ratios. For example, each of the first two integrals (6.3) and (6.4) depend only on a single pair of cross ratios. These are the well-known one-loop and two-loop ladder integrals, which are given by singled-valued polylogarithms [58]

$$F_p(z, \bar{z}) = \sum_{j=0}^p \frac{(-1)^j (2p-j)!}{p! (p-j)! j!} \log(z\bar{z})^j \times \frac{\text{Li}_{2p-j}(z) - \text{Li}_{2p-j}(\bar{z})}{z - \bar{z}}. \quad (6.7)$$

For the two five-point conformal integrals (6.5) and (6.6), no closed-form expressions are known for generic configurations of the five insertion points. However, they have been computed in a particular kinematical regime that will be important for us [59]: The four-dimensional null polygon limit, also known as double light-cone limit. Evaluating the pentagon in this limit is what we turn to now.

6.2 4d Null Polygon Limit

In the four-dimensional null polygon limit, the insertion points of the operators approach the cusps of a four-dimensional null polygon, such that all neighboring points become light-like separated ($x_{i,i+1}^2 \rightarrow 0$). In this limit, all five-point cross-ratios u_i defined in Figure 7 go to zero, $u_i \rightarrow 0$. The conformal integrals develop logarithmic divergences, their leading behavior was computed in [13] and is given by

$$x_{13}^2 x_{24}^2 \mathbb{I}_1^{[1234]} = \ell_5(\ell_1 + \ell_4) + 2\zeta_2, \quad (6.8)$$

$$x_{13}^4 x_{24}^2 \mathbb{I}_5^{[13|24]} = \frac{1}{4} \ell_5^2 (\ell_1^2 + \ell_4)^2 + \frac{1}{2} (\ell_5^2 + 4\ell_5(\ell_1 + \ell_4) + (\ell_1 + \ell_4)^2) \zeta_2 + \frac{21}{2} \zeta_4, \quad (6.9)$$

$$x_{13}^2 x_{14}^2 x_{24}^2 \mathbb{I}_6^{[14|23|5]} = \frac{1}{4} \ell_5 (\ell_1^2 \ell_2 + \ell_3 \ell_4^2 + 2\ell_1 \ell_2 \ell_3 + 2\ell_2 \ell_3 \ell_4) - \frac{1}{2} (\ell_1^2 + \ell_4^2 + 2\ell_1 \ell_3 + 2\ell_2 \ell_4 - 2\ell_2 \ell_5 - 2\ell_3 \ell_5 - 4\ell_2 \ell_3 - 4\ell_1 \ell_5 - 4\ell_4 \ell_5) \zeta_2 + (\ell_2 + \ell_3 - 2\ell_5) \zeta_3 + 5\zeta_4, \quad (6.10)$$

$$x_{13}^2 x_{24}^2 x_{35}^2 \mathbb{I}_7^{[12|34|5]} = \frac{1}{4} \ell_1 \ell_5 (\ell_1 + 2\ell_4) (\ell_5 + 2\ell_2) + (\ell_2 \ell_4 + 2\ell_1 \ell_2 + 2\ell_1 \ell_5 + 2\ell_4 \ell_5) \zeta_2 - (\ell_2 + \ell_4) \zeta_3 + \frac{31}{4} \zeta_4. \quad (6.11)$$

where $\ell_i = \log(u_i)$. Subleading terms will contain powers of u_i and are not included.

In the four-dimensional null polygon limit, we can therefore express the two-loop pentagon (6.2) as a function of the (divergent) logarithms ℓ_i and the finite propagators d_{ij} , which encode the number of internal bridges in the pentagon.

The polygons \mathbb{M}_n are limits of generating functions in the charges of the external operators. As such, the polygons themselves are also generating functions.¹⁷ In order to study the four-dimensional null limit, we further project the polygons down to terms that contain specific powers of propagators d_{ij} on the diagonals (ij) of the polygon. Specifically, we focus on the terms displayed in Figure 7, which are defined as

$$\mathbb{M}_5^{h,k} = \left[\text{coefficient of } (d_{25}^h d_{24}^k) \text{ in } \mathbb{M}_5 \right]_{d_{i,j} \rightarrow 0}. \quad (6.12)$$

The object $\mathbb{M}_5^{h,k}$ is the part of the pentagon \mathbb{M}_5 that has h propagators (or units of R-charge flux, also called ‘‘bridges’’) between operators 2 and 5, and k propagators between operators 2 and 4. The coefficients $\mathbb{M}_5^{h,k}$ were studied earlier [44], and can easily be extracted from (6.2) and be evaluated in the four-dimensional null limit using (6.3)–(6.6). For example, the pentagon with two bridges of length one is given by

$$\begin{aligned} \mathbb{M}_5^{1,1} = 1 - \frac{g^4}{4} & \left(\ell_1^2 (\ell_2 + \ell_5)^2 + \ell_3^2 (\ell_2 + \ell_4)^2 + 2\zeta_2 (\ell_1^2 + 2\ell_2^2 + \ell_3^2 + \ell_4^2 + \ell_5^2 \right. \\ & \left. + 4\ell_1 \ell_2 + 4\ell_2 \ell_3 + 2\ell_2 \ell_4 + 4\ell_3 \ell_4 + 4\ell_1 \ell_5 + 2\ell_2 \ell_5) + 84\zeta_4 \right) + \mathcal{O}(g^6). \end{aligned} \quad (6.13)$$

Notice that due to the factorization property (2.15) of the polygons, the loop corrections to this object only start at $\mathcal{O}(g^4)$. More generally, the pentagon coefficients $\mathbb{M}_5^{h,k}$ will only receive loop corrections at order $g^{2(\min\{h,k\}+1)}$. From this point of view, the pentagon with no internal bridges $\mathbb{M}_5^{0,0}$ is the most non-trivial object, and it has been studied before [13, 34, 40, 41]. In the four-dimension null polygon limit, we find that it exponentiates to

$$\log(\mathbb{M}_5^{0,0}) = -5g^2 \zeta_2 + \frac{135}{4} g^4 \zeta_4 - \sum_{n=1}^5 \left((g^2 - 2g^4 \zeta_2) \ell_n \ell_{n+1} - g^4 \zeta_2 \ell_n (\ell_n + \ell_{n+2}) \right) + \mathcal{O}(g^6), \quad (6.14)$$

which agrees with [13], and with the all-loop conjecture [41] for the null pentagon. In our notation, the latter reads

$$\log(\mathbb{M}_5^{0,0}) = \mathcal{C}_0(g) - \sum_{n=1}^5 \frac{\Gamma_{\text{cusp}}(g)}{4} \ell_n \ell_{n+1} + \frac{\Gamma_{\text{oct}}(g) - \Gamma_{\text{cusp}}(g)}{8} \ell_n (\ell_n + \ell_{n+2}). \quad (6.15)$$

¹⁷The polygon limit projects the full generating function to terms that have large powers of four-dimensional propagators $d_{i,i+1}$ on the perimeter. At five and six points, one can engineer large-charge operators (\mathcal{O}_k and their descendants (2.1)) such that the resulting correlator is exclusively given by the square of the respective polygon. In general, this is not the case: Correlators of operators \mathcal{O}_k , even with k large, will include terms that are squares of polygons, but it will also contain other terms. See the discussion at the end of Section 2.

For comparison, the square $\mathbb{M}_4^{0,0}$ in the four-dimensional null limit expands to

$$\log(\mathbb{M}_4^{0,0}) = \mathcal{D}_0(g) - \sum_{n=1}^2 \frac{\Gamma_{\text{oct}}(g)}{4} \ell_n \ell_{n+1} + \frac{\Gamma_{\text{oct}}}{8} \ell_n (\ell_n + \ell_{n+2}) = -\frac{\Gamma_{\text{oct}}}{4} \log^2\left(\frac{u_1}{u_2}\right), \quad (6.16)$$

where $\ell_i = \log(u_i)$, and $u_1 = u_3 = u$, $u_2 = u_4 = v$. Here, $\mathcal{C}_0(g)$ and $\mathcal{D}_0(g)$ are finite functions of the coupling. The perturbative expansions of the cusp and octagon anomalous dimensions are $\Gamma_{\text{cusp}}(g) = 4g^2 - 8\zeta_2 g^4 + \mathcal{O}(g^6)$ and $\Gamma_{\text{oct}}(g) = 4g^2 - 16\zeta_2 g^4 + \mathcal{O}(g^6)$. Note that our two-loop data can barely distinguish between Γ_{cusp} and Γ_{oct} , thus our result only lends marginal support to the conjecture (6.15). It would be nice to evaluate the pentagon at higher orders in perturbation theory to test this conjecture, and understand if its null limit is controlled by $\Gamma_{\text{cusp}}(g)$ and $\Gamma_{\text{oct}}(g)$, or other tilted cusps $\Gamma_\alpha(g)$, as is the case in the origin limits of gluon scattering amplitudes [60, 61].

6.3 Leading Logarithms

On top of the null polygonal limit, there is another, more simplifying limit that one can consider: The leading logarithm or “stampedes” double-scaling limit [32, 43, 44]. This limit is attained by taking both $g \rightarrow 0$ and $u_i \rightarrow 0$, $i = 1, \dots, 5$, such that the so-called cusp times

$$t_n^2 \equiv g^2 \log(u_{n-2}) \log(u_{n+2}) = g^2 \ell_{n-2} \ell_{n+2} \quad (6.17)$$

are held fixed. This limit projects to the most divergent terms in the four-dimensional null polygon limit, which are the terms with the highest powers of logarithms in (6.8-6.11). For example,

$$g^2 x_{13}^2 x_{24}^2 \mathbb{I}_1^{[1234]} \rightarrow (t_2^2 + t_3^2) \quad \text{and} \quad g^4 x_{13}^2 x_{24}^2 x_{35}^2 \mathbb{I}_7^{[12|34|5]} \rightarrow \frac{(t_3^2 + 2t_2^2)(t_3^2 + 2t_4^2)}{4}. \quad (6.18)$$

Akin to the ordinary four-dimensional null polygon limit, we can also compute the stampedes limit of the pentagons $\mathbb{M}_5^{h,k}$ with arbitrary bridge lengths. For example, for the two cases $\mathbb{M}_5^{0,0}$ and $\mathbb{M}_5^{1,1}$ considered before, the stampedes limit is given by

$$\mathbb{M}_5^{0,0} \rightarrow 1 - (t_1^2 + t_2^2 + t_3^2 + t_4^2 + t_5^2) + \frac{1}{2}(t_1^2 + t_2^2 + t_3^2 + t_4^2 + t_5^2)^2 + \mathcal{O}(t_i^6) \quad (6.19)$$

$$\mathbb{M}_5^{1,1} \rightarrow 1 + (t_3^2 + t_4^2)^2 + (t_1^2 + t_5^2)^2 + \mathcal{O}(t_i^6) \quad (6.20)$$

Remarkably, these two stampedes-limit pentagons are not independent [43]. In fact, all coefficients $\mathbb{M}_5^{h,k}$ in the stampedes limit are related via a set of coupled lattice Toda differential equations, see equation (10) in [44]. The seed of these equations is the empty pentagon $\mathbb{M}_5^{0,0}$, which as we saw already exponentiates in the four-dimensional null polygonal limit, and in the stampedes limit simply becomes

$$\mathbb{M}_5^{0,0} = e^{-(t_1^2 + t_2^2 + t_3^2 + t_4^2 + t_5^2)}. \quad (6.21)$$

The two-loop expression (6.19) of $\mathbb{M}_5^{0,0}$ computed above perfectly reproduces the perturbative expansion of this exponentiation. Moreover, we verified that the pentagon with length-one bridges $\mathbb{M}_5^{1,1}$ as well as all other pentagons $\mathbb{M}_5^{h,k}$ with arbitrary bridge lengths h, k computed from our two-loop result for \mathbb{M}_5 also agree perfectly with the stampedes prediction.

Polygons with Crossing Bridges. Finally, let us address the seemingly non-planar configurations like the ones depicted on the center of [Figure 7](#). Such configurations can be extracted in the exact same way as before via

$$\mathbb{M}_5^{h,k,l,m,n} = \text{coefficient of } (d_{25}^h d_{24}^k d_{13}^l d_{14}^m d_{35}^n) \text{ in } \mathbb{M}_5. \quad (6.22)$$

Even when the bridges $d_{25}^h, \dots, d_{35}^n$ overlap each other, these objects are still planar and thus non-vanishing in perturbation theory, as one can see from their values in the stampedes limit, e.g.

$$\mathbb{M}_5^{2,0,1,0,0} = t_1^2 + t_5^2 - \frac{t_1^2(t_2^2 + 2t_3^2)}{2} - \frac{t_5^2(t_4^2 + 2t_3^2)}{2}, \quad (6.23)$$

$$\mathbb{M}_5^{1,1,1,0,0} = \frac{t_5^2 + 2t_1^2}{2} \frac{t_5^2 + 2t_4^2}{2}. \quad (6.24)$$

This happens because the bridges in (6.22) can be identified one-to-one with contractions of the R-charge polarization vectors $y_i \cdot y_j$ of the operators, but not with color (and spacetime) propagators. At tree-level, each factor d_{ij} is truly a propagator, containing $y_i \cdot y_j$, $1/x_{ij}^2$, and a color propagator factor. Therefore, terms with overlapping d_{ij} factors are truly non-planar, i.e. they vanish at leading order in the planar limit. Beyond tree level, loop corrections can re-route the R-charge flow and change the color structure (as well as the $1/x_{ij}^2$ propagator structure). Thus at loop order, the color structure no longer maps one-to-one to the topology of d_{ij} factors, and terms with overlapping d_{ij} factors may acquire terms that contribute to the leading order in the $1/N_c$ expansion. However, the more the d_{ij} factors overlap, the more loop orders are required for such planar terms to occur. Therefore, the objects (6.22) in the planar limit only start at higher orders in perturbation theory. For example, $\mathbb{M}_5^{1,1,1,0,0}$ starts only at two loops (6.24). We can expect that the pentagon with $h = k = l = m = n = 1$, i.e. all five diagonals present, is only non-zero starting from four loops, which is inaccessible with our present data. And consistently, no such term exists in our two-loop data for \mathbb{M}_5 . To summarize, the pentagon with overlapping bridges is non-planar in internal R-symmetry space, but may be planar in color space. This feature is not restricted to the pentagon, in fact it equally occurs in the square \mathbb{M}_4 , where one can similarly define

$$\mathbb{M}_4^{h,k} = \text{coefficient of } (d_{13}^h d_{24}^k) \text{ in } \mathbb{M}_4, \quad (6.25)$$

and terms with both h and k non-zero are “non-planar” in R-symmetry space. Since the square has disk topology, one cannot think of these two diagonals as existing “inside” and “outside” of the large-R-charge square frame (this may happen for the full four-point correlator with sphere topology). Therefore, all $\mathbb{M}_4^{h,k}$ with $h, k > 0$ are zero at tree level, and only start being non-zero at order $g^{2(h+k-1)}$ in perturbation theory. For example, using the high-loop data of [35], we find

$$\mathbb{M}_4^{1,1} = 0 + t^2 + \frac{t^4}{2} + \frac{t^6}{6} + \frac{5t^8}{144} + \frac{7t^{10}}{1440} + \dots, \quad (6.26)$$

where $t = g^2 \log(z) \log(1-z)$ is the cusp times held fixed. Expanding to higher orders, up to $\mathcal{O}(t^{40})$, and re-summing, we find

$$\mathbb{M}_4^{1,1} = 2t^2 \mathbb{I}_0^2(2t) - 2t^2 \mathbb{I}_1^2(2t) - t \mathbb{I}_0(2t) \mathbb{I}_1(2t), \quad (6.27)$$

where \mathbb{I}_n is the modified Bessel function of the first kind. Interestingly, we find that $\mathbb{M}_4^{1,1}$ is related with square with only one bridge (of size two) via

$$\frac{1}{2t} \frac{d}{dt} \mathbb{M}_4^{1,1} = \mathbb{M}_4^{2,0}. \quad (6.28)$$

It would be nice to further study the stampedes limits of these more general squares and pentagons with crossing bridges $\mathbb{M}_4^{h,k}$ and $\mathbb{M}_5^{h,k,l,m,n}$. The relation above suggests that they might also be related by Toda-like equations, as it happens for polygons with non-crossing bridges $\mathbb{M}_4^{h,0}$ and $\mathbb{M}_5^{h,k,0,0,0}$ [43, 62].

7 Match with Hexagons

The faces decomposition (5.2), together with the one-loop faces (5.11) is reminiscent of the one-loop hexagonalization result [42], but not quite equal to it. According to the hexagonalization proposal [25, 26], the loop corrections to a correlation function of local operators in the planar limit is obtained by dressing each tree-level graph by mirror particles. At one-loop order, the mirror particles are effectively confined to individual faces of the tree-level (ribbon) graphs. However, the sum over mirror particles is not only a function of x_{ij}^2 , but also produces factors d_{ij} that in particular can occur with both positive and also *negative* exponents. The product of d_{ij} factors produced by the underlying tree-level graph thus gets modified to a non-trivial polynomial. In other words, a given monomial (product of d_{ij} factors) in the final answer will receive contributions from different tree-level graphs. Let us see how this works in practice.

The hexagonalization contributions that dress each individual n -point face of each tree graph at one-loop order amount to [25, 42]

$$H_{i_1, \dots, i_n} = 1 + g^2 H_{i_1, \dots, i_n}^{(1)} + \mathcal{O}(g^4),$$

$$H_{i_1, \dots, i_n}^{(1)} = \sum_{k=1}^{n-2} \sum_{m=k+2}^{n-\delta_{k1}} m_{i_k, i_{k+1}, i_m, i_{m+1}}, \quad i_{n+1} \equiv i_1, \quad (7.1)$$

where the sums run over non-overlapping pairs (i_k, i_{k+1}) , (i_m, i_{m+1}) , or equivalently over pairs of non-adjacent edges of the polygonal face. The function m is given by¹⁸

$$m_{ijkl} = \frac{-1}{2x_{i0}^2 x_{j0}^2 x_{k0}^2 x_{l0}^2} \left(x_{il}^2 x_{jk}^2 \left(1 - \frac{d_{il} d_{jk}}{d_{ij} d_{kl}} \right) - x_{ik}^2 x_{jl}^2 \left(1 - \frac{d_{ik} d_{jl}}{d_{ij} d_{kl}} \right) \right). \quad (7.2)$$

The hexagonalization contributions sum to (7.2) integrated over $d^4 x_0$. At one-loop order however, the mapping between the integrated answer and the integrand (7.2) is unambiguous.¹⁹ The function m_{ijkl} has an $S_2 \times S_2$ symmetry:

$$m_{1234} = m_{2143} = m_{3412} = m_{4321}, \quad (7.3)$$

which implies the expected dihedral symmetry for the faces $H_{1, \dots, n}$. In addition, the faces satisfy the “pinching property” [42]

$$H_{\dots, i, j, k, j, l, \dots} = H_{\dots, i, j, l, \dots}. \quad (7.4)$$

As one can see in (7.2), the function m_{ijkl} has factors d_{ij} in the denominator. However, in the combination (7.1), only denominators d_{ij} belonging to the perimeter of the face appear, i. e. $H_{1, \dots, n}$ at most has denominator factors $d_{i, i+1}$, which cancel against the corresponding numerator factors of the ambient tree graph, such that the one-loop correlator is polynomial in $d_{ij} \sim y_{ij}^2$, as required. For example, the one-loop square and pentagon faces become

$$H_{1234}^{(1)} = m_{1234} + m_{2341} \quad (7.5)$$

¹⁸This expression has an overall factor $-1/2$ compared to [42], which is due to differing conventions.

¹⁹Up to parity-odd terms that integrate to zero.

$$\begin{aligned}
&= \frac{1}{2x_{10}^2 x_{20}^2 x_{30}^2 x_{40}^2} \left(x_{13}^2 x_{24}^2 \left(1 - \frac{d_{13}d_{24}}{d_{14}d_{23}} \right) - x_{14}^2 x_{23}^2 \left(1 - \frac{d_{14}d_{23}}{d_{12}d_{34}} \right) + (\text{C}_4 \text{ perms}) \right), \\
H_{12345}^{(1)} &= m_{1234} + m_{1245} + m_{2345} + m_{2351} + m_{3451} \\
&= \frac{x_{13}^2 x_{24}^2}{x_{10}^2 x_{20}^2 x_{30}^2 x_{40}^2} \left(1 - \frac{d_{13}d_{24}}{d_{12}d_{34}} \right) - \frac{x_{14}^2 x_{23}^2}{x_{10}^2 x_{20}^2 x_{30}^2 x_{40}^2} \left(1 - \frac{d_{14}d_{23}}{d_{12}d_{34}} \right) + (\text{C}_5 \text{ perms}).
\end{aligned} \tag{7.6}$$

The one-loop contribution to any correlator is obtained by inserting the one-loop mirror-particle sums $H_{i_1, \dots, i_n}^{(1)}$ into the faces of the tree-level graphs of the respective correlator. Therefore, the complete one-loop generating function $G_{n,1}$ is obtained by inserting the same functions $H_{i_1, \dots, i_n}^{(1)}$ into the faces of the graphs of the tree-level generating function $G_{n,0}$. The edges of the tree-level graphs now produce re-summed (ten-dimensional) propagators $D_{ij} = d_{ij} + d_{ij}^2 + d_{ij}^3 + \dots$. Notably, the structure of the function m_{ijkl} is such that it can produce numerator factors $1 - d_{ij} = D_{ij}/d_{ij}$ when summing over tree graphs. This may affect the ten-dimensional pole structure of the ambient graph, since it can modify the product of $D_{ij} \sim 1/X_{ij}^2$ factors produced by the graph. Consequently, the coefficient of a given D_{ij} product in the final result may receive contributions from several different tree graphs (D_{ij} monomials). For example,

$$\begin{aligned}
(1 + D_{jk})m_{ijkl} &= \frac{m_{ijkl}}{1 - d_{jk}} \\
&= \frac{1}{x_{i0}^2 x_{j0}^2 x_{k0}^2 x_{l0}^2} \left[\frac{d_{il} x_{il}^2 x_{jk}^2}{d_{ij} d_{kl}} + \frac{D_{jk}}{d_{jk}} \left(\left(1 - \frac{d_{il}}{d_{ij} d_{kl}} \right) x_{il}^2 x_{jk}^2 - \left(1 - \frac{d_{ik} d_{jl}}{d_{ij} d_{kl}} \right) x_{ik}^2 x_{jl}^2 \right) \right].
\end{aligned} \tag{7.7}$$

This property makes it slightly non-trivial to match the proposal (5.11) analytically against the prediction from hexagonalization. But by explicit computation, we do find an exact match with $M_{n,1}$ for $n = 4, 5, 6, 7$ by inserting the one-loop faces H_{i_1, \dots, i_m} into the graphs of $M_{n,0}$.²⁰ Moreover, we also find an exact match with the full generating functions $G_{4,1}$, $G_{5,1}$, and $G_{6,1}$ after inserting the one-loop faces into the graphs of the tree-level generating functions $G_{n,0}$.

One might wonder how it can be consistent that inserting the hexagonalization faces H_{i_1, \dots, i_n} into the graphs of $M_{n,0}$ gives the same answer as inserting the one-loop faces $F_{i_1, \dots, i_n}^{(1)}$ (5.11) into the exact same graphs (5.1), even though H_{i_1, \dots, i_n} and $F_{i_1, \dots, i_n}^{(1)}$ are clearly different. The reason for this are the effects discussed below (7.6), and is also related to the ambiguity pointed out in [Footnote 10](#): The two decompositions are related by shifting terms between different faces and/or different graphs. Only the sum over all graphs is the same in both decompositions. The faces \mathbb{F}_n are still unambiguously defined by (5.1) (recursively in n), since for the purpose of defining \mathbb{F}_n , we set $d_{i,i+1} = 0$ in that relation for all $i = 1, \dots, n$.

8 Discussion

Ten-dimensional null polygon correlators are interesting objects for several reasons. They form a middle ground between planar massless scattering amplitudes, for which a rich web of interesting structures and methods have been developed during the past two decades, and correlation functions of single-trace local operators, which are significantly more complicated, in particular due to their sphere topology in color space. The ten-dimensional null polygons \mathbb{M}_n offer a sweet spot: They largely tame the complicated structure of general

²⁰When we do this comparison, we must take the limit $d_{i,i+1} \rightarrow 1$ for $i = 1, \dots, n$ of the one-loop hexagonalization faces H_{i_1, \dots, i_m} , to be consistent with the ten-dimensional polygon limit.

correlation functions by their disk topology, and at the same time offer a natural off-shell generalization of massless amplitudes that is UV and IR finite.

The ten-dimensional null polygons as observables in $\mathcal{N} = 4$ SYM were established in [35]. In this paper, we study the polygon correlators in more depth, in particular pushing their computation in the higher-point case with more than four external operators. Our key results are:

- A method to directly compute the polygons \mathbb{M}_n , which is derived from the twistor rules for general correlators of arbitrary-charge BPS scalar operators [36].
- Explicit formulas for the one-loop and two-loop integrands $M_{n,1}$ and $M_{n,2}$ for any number n of external operators, based on a tessellation of the integrands into faces that are free of ten-dimensional poles.

In the case of massless scattering amplitudes, the determination of the two-loop MHV amplitude for any number of points [57, 63] was an important stepping stone for many later developments and discoveries. One may hope that many of the structures found for massless amplitudes will have generalizations for the polygons \mathbb{M}_n . Let us highlight some of the potential directions, many of which are interrelated:

Massive Amplitudes. There is evidence that the polygon correlators are dual to massive scattering amplitudes on the Coulomb branch of $\mathcal{N} = 4$ SYM, which extends the massless amplitude/correlator duality to an off-shell setting [35].

In the 4d massless limit, the *integrands* $M_{n,\ell}$ reduce to the ℓ -loop integrands of 4d null correlators of **20'** operators, which equal the integrands of massless MHV gluon amplitudes (2.16). However, this limit does not commute with the integration over the Lagrangian points. In particular, when taking the massless limit of the integrated \mathbb{M}_n , its divergences (Sudakov logarithms) are no longer governed by the cusp anomalous dimension Γ_{cusp} of massless amplitudes, but instead by the *octagon anomalous dimension* Γ_{oct} [32]. This was first observed for the square [35], and later for the pentagon [13].²¹

Prompted by the proposed off-shell correlator/amplitude duality [35], five-point and six-point amplitudes of massive W-bosons on the Coulomb branch have been computed [40, 41, 64]. For the five-point amplitude, it was found that its infrared divergences in the on-shell (massless) limit are governed by the octagon anomalous dimension [40], which generalizes the four point result [35]. Moreover, the five-point amplitudes equals the pentagon correlator in the double-scaling “stampedes” limit [41]. These results further corroborate the proposed off-shell duality.

However, a full match between off-shell Coulomb-branch amplitudes and polygon correlators beyond four points is still missing. The duality is not yet fully formulated, because we lack a clear organizational principle of the amplitude polarizations. The latter would be required for a precise dictionary, which could then be tested (even at integrand level). Speaking in terms of massless concepts, we are missing the analog of MHV and N^k MHV amplitudes in the massive case.

In its firmly established massless incarnation, the duality between correlation functions and gluon amplitudes is in fact a *triality* that also includes null polygon Wilson loops [16, 19, 20, 65–67]. Going off-shell, could there be a Wilson-loop-like object that provides a bridge between polygon correlators and Coulomb-branch amplitudes? For first steps in this direction, see [68].

²¹Intriguingly, the octagon anomalous dimension also governs gluon amplitudes in the “origin limit” [60, 61].

Recursion Relations. The 10d all-loop factorization (2.15) is reminiscent of an amplitude factorization on an on-shell particle with momentum x_{ij}^μ and mass $m^2 = -y_{ij}^2$. This lends motivation to look for generalizations of off-shell Berends–Giele [69] or on-shell BCFW [70, 71] recursion relations to the polygon correlators. The factorization poles (2.15) are completely on-shell (from a 10d perspective). Can one engineer a holomorphic deformation of the kinematics, such that the pole at infinity can be systematically understood?

Correlahedron. It would be interesting to see if there is a geometric description for the polygon integrands, like the amplituhedron for massless amplitudes [72], and the correlahedron for stress-energy correlators [73]. The relation of the polygon correlators to Coulomb-branch amplitudes indicates that such a description could exist. A geometric description could also single out a particular integrand form (like the dlog forms in the massless case), which could in turn help find good master integrals, or even better a good finite function space that one could use for a functional bootstrap of the integrated polygons. A possible starting point in the search of such a description could be the recently proposed “deformed” amplituhedron [74] whose parameters can be interpreted as vacuum expectation values on the Coulomb branch. As a first step, one could look for a parametrization of the square correlator (a. k. a. octagon) that matches the two-loop integrand/amplitude of [74], and then study the resulting geometry in this parametrization.

Superpolygons & 10d Symmetry. The bosonic polygon correlators \mathbb{M}_n should have supersymmetric generalizations where $4(n - 4)$ Grassmann variables θ are distributed on the perimeter of the polygon. Some information on this supersymmetrization could be derived by taking the n -point ten-dimensional null limit of the m -point generating function $G_{m,\ell}$, with $m < n$. However, this would require to also include all higher Kaluza–Klein modes of $(n - m)$ of the Lagrangian insertion points in the generating function, which has presently only been done for $m = 4$, i. e. the square [35].

The proposed superpolygon correlator should naturally decompose into basic superconformal invariants. In fact, this decomposition should derive from a corresponding decomposition of the full super-generating function (before taking the ten-dimensional null limit). At four points, there is only one such superinvariant \mathcal{R} [1]. In the ℓ -loop integrands of four **20'** operators, \mathcal{R} absorbs all dependence on the polarizations y_i , hence its coefficient function \mathcal{H} (the “reduced correlator”) is a function of x_{ij}^2 only. And in fact, the full four-point generating functions $G_{4,\ell}$ (including all KK modes of the Lagrangian) are obtained by promoting all four-dimensional x_{ij}^2 in the reduced correlator \mathcal{H} to ten-dimensional X_{ij}^2 , which results in a ten-dimensional conformal symmetry [35]. Projecting $G_{4,\ell}$ to the square correlator $M_{4,\ell}$, this structure is preserved: The remnant of \mathcal{R} (3.10) is multiplied by a function with ten-dimensional conformal symmetry (3.4).

One can expect that this structure repeats at higher points, only that now there will be several superinvariants, each multiplied by a different 10d-symmetric “reduced correlator”. The decomposition into superinvariants is not known even at five points, which makes it difficult to look for ten-dimensional symmetry. However, the pentagon correlator already has a suggestive form (3.13): Two structures p and q multiply combinations of conformal integrands that could be promoted to functions with 10d symmetry (conjecturally including the higher KK modes of the Lagrangian points). Further supporting evidence for the existence of such a decomposition derives from

strong coupling, where the five-point correlator in supergravity could be organized over 10d denominators, with coefficients that are linear combinations of superinvariants [38].

Better understanding the decomposition into superinvariants would also help make the duality with Coulomb-branch amplitudes more precise. This was the case for the massless correlator/amplitude duality: The super Wilson-loop defined in [21, 22] allowed for a complete duality including all N^k MHV massless amplitudes [48].

Integrability. Correlation functions of local operators can be computed from integrability by decomposing them into hexagon form factors [24–26]. Performing such computations in practice is difficult due to the intricate interactions among all contributing worldsheet excitations, and in particular due to winding modes that require careful treatment [49]. Polygon correlators have disk topology and thus admit no non-trivial cycles, hence winding modes are projected out, which should simplify their computation. In this sense, the polygons \mathbb{M}_n are the most natural objects one can compute from hexagons. In fact the hexagonalization of the square (a. k. a. octagon) led to an all-loop [29–31] and even finite-coupling resummation [32, 33].

It would be great to study the dynamics of worldsheet excitations on the polygon correlators in more depth. The present formalism admitted the computation of the pentagon to two loops [34], but is plagued by a complicated matrix structure. Can one find a more suitable basis of excitations that is specifically tailored for polygon computations, and that makes the sum over excitations “more diagonal”? Perhaps in simplifying kinematic limits?

Of particularly interest is the four-dimensional null limit, in which one can expect some similarity with the pentagon OPE for massless amplitudes (null polygon Wilson loops) [50–53]. The two will not be the same, as one can already see from their distinct anomalous dimensions (Γ_{cusp} vs. Γ_{oct}). Moreover, massless amplitudes have no R-charge flowing around their perimeter, whereas the polygon correlators are surrounded by a large charge flow. It would be great to understand the differences and similarities of the pentagon OPE and the hexagon expansion in the massless limit in more detail.

Further input can come from strong coupling: The square correlator could be computed from a clustering procedure [75, 76]. Can the same be done for bigger polygons? The square is described by an integral over a single Y-function [76]. Is there a Y-system for strongly coupled polygons, similar to the massless amplitude case [77]?

Integration & Functional Bootstrap. In this work, we have focused on the integrands $M_{n,\ell}$ of the polygon correlators. Of course it would be interesting to integrate over the Lagrangian points to obtain the fully interacting n -point polygons \mathbb{M}_n . For the square, this was possible because the result is exclusively expressed in terms of well-known ladder integrals [29]. At higher points, the situation is very different. There have been some recent advances in computing five-point and six-point loop integrals [13, 78–86], but the completely off-shell higher-point integrals remain mostly unknown, hence a direct integration looks infeasible at the moment.

A more promising route to the integrated polygons would be a functional bootstrap, which has been applied very successfully in the massless amplitude case (see e. g. [87] for a review). The first requisite for this would be the knowledge of the leading singularities as well as the symbol alphabet (assuming that the polygons are expressible in terms of multiple polylogarithms). At five points, it might be feasible to extract this information, for example by relating the occurring integrals to non-conformal off-shell

four-point integrals [88]. Once the function space is known (e.g. leading singularities and alphabet), one could write a linear ansatz at each loop order, and fix all remaining freedom by boundary data from hexagonalization.

Yangian Symmetry. The polygons are cyclically invariant objects with disk topology, hence one might expect that they (or their supersymmetric generalizations) transform in some realization of the $\mathfrak{psu}(2, 2|4)$ Yangian symmetry of $\mathcal{N} = 4$ super Yang–Mills theory. In the case of massless amplitudes, the space of invariants is strongly reduced by Yangian symmetry in the form of dual superconformal invariance, which greatly facilitates their construction. Could Yangian symmetry play a similar role for the polygon correlators considered here?

We hope that the large amount of data provided in this work will help to address some of these interesting questions in the future.

Acknowledgments

We thank Benjamin Basso, Simon Caron-Huot, Thiago Fleury, Johannes Henn, Paul Heslop, Gregory Korchemsky, Davide Lai, and Tabea Siebrecht for interesting discussions. The work of T. B., A. B., and C. B. was funded by the Deutsche Forschungsgemeinschaft (DFG, German Research Foundation) Grant No. 460391856. T. B., A. B., and C. B. acknowledge support from DESY (Hamburg, Germany), a member of the Helmholtz Association HGF, and by the Deutsche Forschungsgemeinschaft (DFG, German Research Foundation) under Germany’s Excellence Strategy – EXC 2121 “Quantum Universe” – 390833306. A. B. is further supported by the Studienstiftung des Deutschen Volkes. The work of F.C. is supported in part by the Simons Foundation grant 994306 (Simons Collaboration on Confinement and QCD Strings), as well the NCCR SwissMAP that is also funded by the Swiss National Science Foundation.

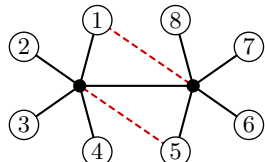
A Two-Loop Faces in Terms of Conformal Integrals

In Section 5.3, we decomposed the two-loop faces $F_{1,\dots,n}^{(2)}$ into a basis of three different propagator structures \mathcal{J}_1 , \mathcal{J}_2 , and \mathcal{J}_3 that are free of numerator factors. In other words, all numerator factors are absorbed in the coefficients $f_{k,e,a,b}$ of that decomposition (5.13). Alternatively, and perhaps more naturally if one aims for actually integrating over the Lagrangian points, is to keep all dependence on the Lagrangian insertion points together, and expand in a rational basis of integrands \mathcal{I}_k of planar conformal integrals:

$$F_{1,\dots,n}^{(2)} = \sum_{k,e} \tilde{f}_{k,e}(x_{ij}^2, y_{ij}^2) \mathcal{I}_k^e + (\text{D}_n \text{ perms}), \quad (\text{A.1})$$

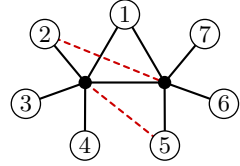
where the sum over k runs over the 12 different conformal integrands \mathcal{I}_k that appear, e labels their planar embeddings in the face $F_{1,\dots,n}$, and $\tilde{f}_{k,e}$ are rational coefficients that only depend on the spacetime distances x_{ij}^2 and internal (R-charge) distances y_{ij}^2 among the external points $1, \dots, n$.

In order to list the conformal integrands that appear, we define the following eight-point double-pentagon “master” integrand:

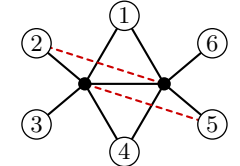


$$\mathcal{I}_1^{1,\dots,8,a,b} = \frac{1}{2} \left(\frac{x_{1b}^2 x_{5a}^2}{x_{1a}^2 x_{2a}^2 x_{3a}^2 x_{4a}^2 x_{ab}^2 x_{5b}^2 x_{6b}^2 x_{7b}^2 x_{8b}^2} + (a \leftrightarrow b) \right) \quad (\text{A.2})$$

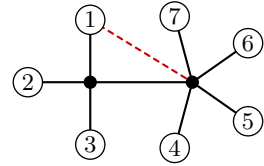
All two-loop integral topologies that appear in the decomposition (A.1) can be obtained from permutations and limits of this master integrand:



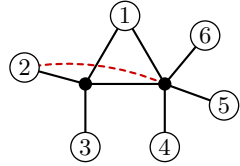
$$\mathcal{I}_2^{1,\dots,7,a,b} = \mathcal{I}_1^{2,1,3,4,5,6,7,1,a,b}, \quad (\text{A.3})$$



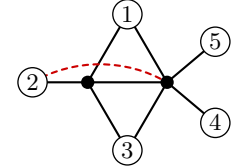
$$\mathcal{I}_3^{1,\dots,6,a,b} = \mathcal{I}_1^{2,1,3,4,5,4,6,1,a,b}, \quad (\text{A.4})$$



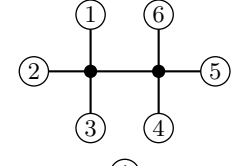
$$\mathcal{I}_4^{1,\dots,7,a,b} = \mathcal{I}_1^{1,2,3,4,4,5,6,7,a,b}, \quad (\text{A.5})$$



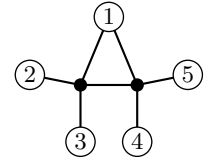
$$\mathcal{I}_5^{1,\dots,6,a,b} = \mathcal{I}_1^{2,1,3,4,4,5,6,1,a,b}, \quad (\text{A.6})$$



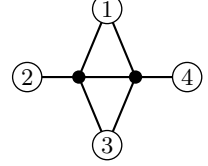
$$\mathcal{I}_6^{1,\dots,5,a,b} = \mathcal{I}_1^{2,1,3,3,3,4,5,1,a,b}, \quad (\text{A.7})$$



$$\mathcal{I}_7^{1,\dots,6,a,b} = \mathcal{I}_1^{1,2,3,4,4,5,6,1,a,b}, \quad (\text{A.8})$$

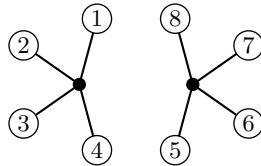


$$\mathcal{I}_8^{1,\dots,5,a,b} = \mathcal{I}_1^{1,2,3,4,4,5,1,1,a,b}, \quad (\text{A.9})$$

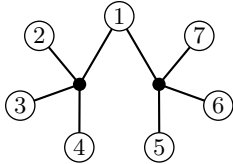


$$\mathcal{I}_9^{1,\dots,4,a,b} = \mathcal{I}_1^{1,2,3,3,3,4,1,1,a,b}. \quad (\text{A.10})$$

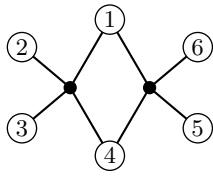
\mathcal{I}_1 , \mathcal{I}_2 , and \mathcal{I}_3 are the eight-point, seven-point, and six-point double-penta integrands. \mathcal{I}_4 , \mathcal{I}_5 , and \mathcal{I}_6 are the seven-point, six-point, and five-point penta-box integrands. And \mathcal{I}_7 , \mathcal{I}_8 , and \mathcal{I}_9 are the six-point, five-point, and four-point double-box integrands. Besides these two-loop integrands, the following products of one-loop box integrands also contribute to (A.1):



$$\mathcal{I}_{10}^{1,\dots,8,a,b} = \frac{1}{2} \left(\frac{1}{x_{1a}^2 x_{2a}^2 x_{3a}^2 x_{4a}^2} \frac{1}{x_{5b}^2 x_{6b}^2 x_{7b}^2 x_{8b}^2} + (a \leftrightarrow b) \right), \quad (\text{A.11})$$



$$\mathcal{I}_{11}^{1,...,7,a,b} = \mathcal{I}_{10}^{1,2,3,4,5,6,7,1,a,b}, \quad (\text{A.12})$$



$$\mathcal{I}_{12}^{1,...,6,a,b} = \mathcal{I}_{10}^{1,2,3,4,4,5,6,1,a,b}. \quad (\text{A.13})$$

The coefficient functions $\tilde{f}_{k,e}$ are functions of the spacetime and internal distances. They depend polynomially on the internal distances y_{ij}^2 . Their dependence is further constrained by the fact that the faces $F_{1,...,n}$ are conformally invariant functions of x_i when expressed in terms of d_{ij} and x_{ij}^2 . Most importantly, $F_{1,...,n}$ reduce to the integrand of the massless n -point gluon amplitude [57] in the $y_i \rightarrow 0$ limit (2.16).

References

- [1] B. Eden, P. Heslop, G. P. Korchemsky and E. Sokatchev, *Hidden symmetry of four-point correlation functions and amplitudes in $\mathcal{N} = 4$ SYM*, *Nucl. Phys. B* **862**, 193 (2012), [arxiv:1108.3557](https://arxiv.org/abs/1108.3557).
- [2] J. Drummond, C. Duhr, B. Eden, P. Heslop, J. Pennington and V. A. Smirnov, *Leading singularities and off-shell conformal integrals*, *JHEP* **1308**, 133 (2013), [arxiv:1303.6909](https://arxiv.org/abs/1303.6909).
- [3] G. Arutyunov and S. Frolov, *Four point functions of lowest weight CPOs in $\mathcal{N} = 4$ SYM(4) in supergravity approximation*, *Phys. Rev. D* **62**, 064016 (2000), [hep-th/0002170](https://arxiv.org/abs/hep-th/0002170).
- [4] V. Gonçalves, *Four point function of $\mathcal{N} = 4$ stress-tensor multiplet at strong coupling*, *JHEP* **1504**, 150 (2015), [arxiv:1411.1675](https://arxiv.org/abs/1411.1675).
- [5] L. F. Alday and T. Hansen, *The AdS Virasoro-Shapiro amplitude*, *JHEP* **2310**, 023 (2023), [arxiv:2306.12786](https://arxiv.org/abs/2306.12786).
- [6] N. Drukker and J. Plefka, *The Structure of n -point functions of chiral primary operators in $\mathcal{N} = 4$ super Yang–Mills at one-loop*, *JHEP* **0904**, 001 (2009), [arxiv:0812.3341](https://arxiv.org/abs/0812.3341).
- [7] T. Bargheer, T. Fleury and V. Gonçalves, *Higher-Point Integrands in $\mathcal{N} = 4$ super Yang–Mills Theory*, *SciPost Phys.* **15**, 059 (2023), [arxiv:2212.03773](https://arxiv.org/abs/2212.03773).
- [8] V. Gonçalves, R. Pereira and X. Zhou, *20' Five-Point Function from $AdS_5 \times S^5$ Supergravity*, *JHEP* **1910**, 247 (2019), [arxiv:1906.05305](https://arxiv.org/abs/1906.05305).
- [9] V. Gonçalves, M. Nocchi and X. Zhou, *Dissecting supergraviton six-point function with lightcone limits and chiral algebra*, *JHEP* **2506**, 173 (2025), [arxiv:2502.10269](https://arxiv.org/abs/2502.10269).
- [10] B. Eden, P. Heslop, G. P. Korchemsky, V. A. Smirnov and E. Sokatchev, *Five-loop Konishi in $\mathcal{N} = 4$ SYM*, *Nucl. Phys. B* **862**, 123 (2012), [arxiv:1202.5733](https://arxiv.org/abs/1202.5733).
- [11] B. Eden, *Three-loop universal structure constants in $\mathcal{N} = 4$ susy Yang–Mills theory*, [arxiv:1207.3112](https://arxiv.org/abs/1207.3112).
- [12] C. Bercini, V. Gonçalves, A. Homrich and P. Vieira, *The Wilson loop — large spin OPE dictionary*, *JHEP* **2207**, 079 (2022), [arxiv:2110.04364](https://arxiv.org/abs/2110.04364).
- [13] C. Bercini, B. Fernandes and V. Gonçalves, *Two-loop five-point integrals: light, heavy and large-spin correlators*, *JHEP* **2410**, 242 (2024), [arxiv:2401.06099](https://arxiv.org/abs/2401.06099).
- [14] T. Bargheer, A. Bekov, C. Bercini and F. Coronado, *Higher-Point Correlators in $\mathcal{N} = 4$ SYM: Generating Functions*, [arxiv:2509.14332](https://arxiv.org/abs/2509.14332).

- [15] L. F. Alday, B. Eden, G. P. Korchemsky, J. Maldacena and E. Sokatchev, *From correlation functions to Wilson loops*, **JHEP** **1109**, 123 (2011), [arxiv:1007.3243](#).
- [16] L. F. Alday and J. M. Maldacena, *Gluon scattering amplitudes at strong coupling*, **JHEP** **0706**, 064 (2007), [arxiv:0705.0303](#).
- [17] N. Berkovits and J. Maldacena, *Fermionic T-Duality, Dual Superconformal Symmetry, and the Amplitude/Wilson Loop Connection*, **JHEP** **0809**, 062 (2008), [arxiv:0807.3196](#).
- [18] N. Beisert, R. Ricci, A. A. Tseytlin and M. Wolf, *Dual Superconformal Symmetry from $AdS_5 \times S^5$ Superstring Integrability*, **Phys. Rev. D** **78**, 126004 (2008), [arxiv:0807.3228](#).
- [19] Z. Bern, L. J. Dixon, D. A. Kosower, R. Roiban, M. Spradlin, C. Vergu and A. Volovich, *The Two-Loop Six-Gluon MHV Amplitude in Maximally Supersymmetric Yang–Mills Theory*, **Phys. Rev. D** **78**, 045007 (2008), [arxiv:0803.1465](#).
- [20] J. M. Drummond, J. Henn, G. P. Korchemsky and E. Sokatchev, *Hexagon Wilson loop = six-gluon MHV amplitude*, **Nucl. Phys. B** **815**, 142 (2009), [arxiv:0803.1466](#).
- [21] L. Mason and D. Skinner, *The Complete Planar S-matrix of $\mathcal{N} = 4$ SYM as a Wilson Loop in Twistor Space*, **JHEP** **1012**, 018 (2010), [arxiv:1009.2225](#).
- [22] S. Caron-Huot, *Notes on the scattering amplitude / Wilson loop duality*, **JHEP** **1107**, 058 (2011), [arxiv:1010.1167](#).
- [23] B. Eden, G. P. Korchemsky and E. Sokatchev, *From correlation functions to scattering amplitudes*, **JHEP** **1112**, 002 (2011), [arxiv:1007.3246](#).
- [24] B. Basso, S. Komatsu and P. Vieira, *Structure Constants and Integrable Bootstrap in Planar $\mathcal{N} = 4$ SYM Theory*, [arxiv:1505.06745](#).
- [25] T. Fleury and S. Komatsu, *Hexagonalization of Correlation Functions*, **JHEP** **1701**, 130 (2017), [arxiv:1611.05577](#).
- [26] B. Eden and A. Sfondrini, *Tessellating cushions: four-point functions in $\mathcal{N} = 4$ SYM*, **JHEP** **1710**, 098 (2017), [arxiv:1611.05436](#).
- [27] T. Fleury and S. Komatsu, *Hexagonalization of Correlation Functions II: Two-Particle Contributions*, **JHEP** **1802**, 177 (2018), [arxiv:1711.05327](#).
- [28] F. Coronado, *Perturbative Four-Point Functions in Planar $\mathcal{N} = 4$ SYM from Hexagonalization*, **JHEP** **1901**, 056 (2019), [arxiv:1811.00467](#).
- [29] F. Coronado, *Bootstrapping the simplest correlator in planar $\mathcal{N} = 4$ SYM at all loops*, **Phys. Rev. Lett.** **124**, 171601 (2020), [arxiv:1811.03282](#).
- [30] I. Kostov, V. B. Petkova and D. Serban, *Determinant formula for the octagon form factor in $\mathcal{N} = 4$ SYM*, **Phys. Rev. Lett.** **122**, 231601 (2019), [arxiv:1903.05038](#).
- [31] I. Kostov, V. B. Petkova and D. Serban, *The Octagon as a Determinant*, **JHEP** **1911**, 178 (2019), [arxiv:1905.11467](#).
- [32] A. V. Belitsky and G. P. Korchemsky, *Exact null octagon*, **JHEP** **2005**, 070 (2020), [arxiv:1907.13131](#).
- [33] A. V. Belitsky and G. P. Korchemsky, *Octagon at finite coupling*, **JHEP** **2007**, 219 (2020), [arxiv:2003.01121](#).
- [34] T. Fleury and V. Gonçalves, *Decagon at Two Loops*, **JHEP** **2007**, 030 (2020), [arxiv:2004.10867](#).
- [35] S. Caron-Huot and F. Coronado, *Ten dimensional symmetry of $\mathcal{N} = 4$ SYM correlators*, **JHEP** **2203**, 151 (2022), [arxiv:2106.03892](#).
- [36] S. Caron-Huot, F. Coronado and B. Mühlmann, *Determinants in self-dual $\mathcal{N} = 4$ SYM and twistor space*, **JHEP** **2308**, 008 (2023), [arxiv:2304.12341](#).

[37] S. Caron-Huot and A.-K. Trinh, *All tree-level correlators in $AdS_5 \times S_5$ supergravity: hidden ten-dimensional conformal symmetry*, *JHEP* **1901**, 196 (2019), [arxiv:1809.09173](https://arxiv.org/abs/1809.09173).

[38] B. Fernandes, V. Gonçalves, Z. Huang, Y. Tang, J. Vilas Boas and E. Y. Yuan, *$AdS \times S$ Mellin Bootstrap, Hidden 10d Symmetry and Five-point Kaluza-Klein Functions in $\mathcal{N} = 4$ SYM*, [arxiv:2507.14124](https://arxiv.org/abs/2507.14124).

[39] X.-E. Du, Z. Huang, B. Wang, E. Y. Yuan and X. Zhou, *Meson correlators in 4d $\mathcal{N} = 2$ SCFTs and hints for 8d structures at weak coupling*, *JHEP* **2504**, 128 (2025), [arxiv:2412.17260](https://arxiv.org/abs/2412.17260).

[40] L. V. Bork, N. B. Muzhichkov and E. S. Sozinov, *Infrared properties of five-point massive amplitudes in $\mathcal{N} = 4$ SYM on the Coulomb branch*, *JHEP* **2208**, 173 (2022), [arxiv:2201.08762](https://arxiv.org/abs/2201.08762).

[41] A. V. Belitsky, L. V. Bork, R. N. Lee, A. I. Onishchenko and V. A. Smirnov, *Five W-boson amplitude = near-null decagon*, [arxiv:2510.16471](https://arxiv.org/abs/2510.16471).

[42] T. Bargheer, J. Caetano, T. Fleury, S. Komatsu and P. Vieira, *Handling handles. Part II. Stratification and Data Analysis*, *JHEP* **1811**, 095 (2018), [arxiv:1809.09145](https://arxiv.org/abs/1809.09145).

[43] E. Olivucci and P. Vieira, *Stampedes I: fishnet OPE and octagon Bootstrap with nonzero bridges*, *JHEP* **2207**, 017 (2022), [arxiv:2111.12131](https://arxiv.org/abs/2111.12131).

[44] E. Olivucci and P. Vieira, *Null Polygons in Conformal Gauge Theory*, *Phys. Rev. Lett.* **129**, 221601 (2022), [arxiv:2205.04476](https://arxiv.org/abs/2205.04476).

[45] B. Eden, G. P. Korchemsky and E. Sokatchev, *More on the duality correlators/amplitudes*, *Phys. Lett. B* **709**, 247 (2012), [arxiv:1009.2488](https://arxiv.org/abs/1009.2488).

[46] T. Adamo, M. Bullimore, L. Mason and D. Skinner, *A Proof of the Supersymmetric Correlation Function / Wilson Loop Correspondence*, *JHEP* **1108**, 076 (2011), [arxiv:1103.4119](https://arxiv.org/abs/1103.4119).

[47] B. Eden, P. Heslop, G. P. Korchemsky and E. Sokatchev, *The super-correlator/super-amplitude duality: Part II*, *Nucl. Phys. B* **869**, 378 (2013), [arxiv:1103.4353](https://arxiv.org/abs/1103.4353).

[48] B. Eden, P. Heslop, G. P. Korchemsky and E. Sokatchev, *The super-correlator/super-amplitude duality: Part I*, *Nucl. Phys. B* **869**, 329 (2013), [arxiv:1103.3714](https://arxiv.org/abs/1103.3714).

[49] B. Basso, V. Gonçalves, S. Komatsu and P. Vieira, *Gluing Hexagons at Three Loops*, *Nucl. Phys. B* **907**, 695 (2016), [arxiv:1510.01683](https://arxiv.org/abs/1510.01683).

[50] B. Basso, A. Sever and P. Vieira, *Spacetime and Flux Tube S-Matrices at Finite Coupling for $\mathcal{N} = 4$ Supersymmetric Yang–Mills Theory*, *Phys. Rev. Lett.* **111**, 091602 (2013), [arxiv:1303.1396](https://arxiv.org/abs/1303.1396).

[51] B. Basso, A. Sever and P. Vieira, *Space-time S-matrix and Flux tube S-matrix II. Extracting and Matching Data*, *JHEP* **1401**, 008 (2014), [arxiv:1306.2058](https://arxiv.org/abs/1306.2058).

[52] B. Basso, A. Sever and P. Vieira, *Space-time S-matrix and Flux-tube S-matrix III. The two-particle contributions*, *JHEP* **1408**, 085 (2014), [arxiv:1402.3307](https://arxiv.org/abs/1402.3307).

[53] B. Basso, A. Sever and P. Vieira, *Space-time S-matrix and Flux-tube S-matrix IV. Gluons and Fusion*, *JHEP* **1409**, 149 (2014), [arxiv:1407.1736](https://arxiv.org/abs/1407.1736).

[54] T. Bargheer, F. Coronado and P. Vieira, *Octagons I: Combinatorics and Non-Planar Resummations*, *JHEP* **1908**, 162 (2019), [arxiv:1904.00965](https://arxiv.org/abs/1904.00965).

[55] T. Bargheer, J. Caetano, T. Fleury, S. Komatsu and P. Vieira, *Handling Handles: Nonplanar Integrability in $\mathcal{N} = 4$ Supersymmetric Yang–Mills Theory*, *Phys. Rev. Lett.* **121**, 231602 (2018), [arxiv:1711.05326](https://arxiv.org/abs/1711.05326).

[56] E. Krasko and A. Omelchenko, *Brown's Theorem and its Application for Enumeration of Dissections and Planar Trees*, *The Electronic Journal of Combinatorics* 22, 1.17 (2015).

[57] C. Vergu, *The Two-loop MHV amplitudes in $\mathcal{N} = 4$ supersymmetric Yang–Mills theory*, *Phys. Rev. D* 80, 125025 (2009), [arxiv:0908.2394](https://arxiv.org/abs/0908.2394).

[58] N. I. Ussyukina and A. I. Davydychev, *Exact results for three- and four-point ladder diagrams with an arbitrary number of rungs*, *Phys. Lett. B* 305, 136 (1993).

[59] C. Bercini, V. Gonçalves and P. Vieira, *Light-Cone Bootstrap of Higher Point Functions and Wilson Loop Duality*, *Phys. Rev. Lett.* 126, 121603 (2021), [arxiv:2008.10407](https://arxiv.org/abs/2008.10407).

[60] B. Basso, L. J. Dixon and G. Papathanasiou, *Origin of the Six-Gluon Amplitude in Planar $\mathcal{N} = 4$ Supersymmetric Yang–Mills Theory*, *Phys. Rev. Lett.* 124, 161603 (2020), [arxiv:2001.05460](https://arxiv.org/abs/2001.05460).

[61] B. Basso, L. J. Dixon, Y.-T. Liu and G. Papathanasiou, *All-Orders Quadratic-Logarithmic Behavior for Amplitudes*, *Phys. Rev. Lett.* 130, 111602 (2023), [arxiv:2211.12555](https://arxiv.org/abs/2211.12555).

[62] A. V. Belitsky and G. P. Korchemsky, *Crossing bridges with strong Szegő limit theorem*, *JHEP* 2104, 257 (2021), [arxiv:2006.01831](https://arxiv.org/abs/2006.01831).

[63] S. Caron-Huot, *Superconformal symmetry and two-loop amplitudes in planar $\mathcal{N} = 4$ super Yang–Mills*, *JHEP* 1112, 066 (2011), [arxiv:1105.5606](https://arxiv.org/abs/1105.5606).

[64] A. V. Belitsky, *Towards six W-boson amplitude at two loops*, [arxiv:2511.20828](https://arxiv.org/abs/2511.20828).

[65] L. F. Alday and J. Maldacena, *Comments on gluon scattering amplitudes via AdS/CFT*, *JHEP* 0711, 068 (2007), [arxiv:0710.1060](https://arxiv.org/abs/0710.1060).

[66] J. M. Drummond, G. P. Korchemsky and E. Sokatchev, *Conformal properties of four-gluon planar amplitudes and Wilson loops*, *Nucl. Phys. B* 795, 385 (2008), [arxiv:0707.0243](https://arxiv.org/abs/0707.0243).

[67] A. Brandhuber, P. Heslop and G. Travaglini, *MHV Amplitudes in $\mathcal{N} = 4$ Super Yang–Mills and Wilson Loops*, *Nucl. Phys. B* 794, 231 (2008), [arxiv:0707.1153](https://arxiv.org/abs/0707.1153).

[68] A. V. Belitsky and V. A. Smirnov, *An off-shell Wilson loop*, *JHEP* 2304, 071 (2023), [arxiv:2110.13206](https://arxiv.org/abs/2110.13206).

[69] F. A. Berends and W. T. Giele, *Recursive Calculations for Processes with n Gluons*, *Nucl. Phys. B* 306, 759 (1988).

[70] R. Britto, F. Cachazo and B. Feng, *New recursion relations for tree amplitudes of gluons*, *Nucl. Phys. B* 715, 499 (2005), [hep-th/0412308](https://arxiv.org/abs/hep-th/0412308).

[71] R. Britto, F. Cachazo, B. Feng and E. Witten, *Direct proof of tree-level recursion relation in Yang–Mills theory*, *Phys. Rev. Lett.* 94, 181602 (2005), [hep-th/0501052](https://arxiv.org/abs/hep-th/0501052).

[72] N. Arkani-Hamed and J. Trnka, *The Amplituhedron*, *JHEP* 1410, 30 (2014), [arxiv:1312.2007](https://arxiv.org/abs/1312.2007).

[73] B. Eden, P. Heslop and L. Mason, *The Correlahedron*, *JHEP* 1709, 156 (2017), [arxiv:1701.00453](https://arxiv.org/abs/1701.00453).

[74] N. Arkani-Hamed, W. Flieger, J. M. Henn, A. Schreiber and J. Trnka, *Coulomb Branch Amplitudes from a Deformed Amplituhedron Geometry*, *Phys. Rev. Lett.* 132, 211601 (2024), [arxiv:2311.10814](https://arxiv.org/abs/2311.10814).

[75] Y. Jiang, S. Komatsu, I. Kostov and D. Serban, *Clustering and the Three-Point Function*, *J. Phys. A* 49, 454003 (2016), [arxiv:1604.03575](https://arxiv.org/abs/1604.03575).

[76] T. Bargheer, F. Coronado and P. Vieira, *Octagons II: Strong Coupling*, [arxiv:1909.04077](https://arxiv.org/abs/1909.04077).

[77] L. F. Alday, J. Maldacena, A. Sever and P. Vieira, *Y-system for Scattering Amplitudes*, *J. Phys. A* 43, 485401 (2010), [arxiv:1002.2459](https://arxiv.org/abs/1002.2459).

[78] S. Abreu, H. Ita, F. Moriello, B. Page, W. Tschernow and M. Zeng, *Two-Loop Integrals for Planar Five-Point One-Mass Processes*, **JHEP** **2011**, 117 (2020), [arxiv:2005.04195](https://arxiv.org/abs/2005.04195).

[79] D. D. Canko, C. G. Papadopoulos and N. Syrrakos, *Analytic representation of all planar two-loop five-point Master Integrals with one off-shell leg*, **JHEP** **2101**, 199 (2021), [arxiv:2009.13917](https://arxiv.org/abs/2009.13917).

[80] S. Abreu, H. Ita, B. Page and W. Tschernow, *Two-loop hexa-box integrals for non-planar five-point one-mass processes*, **JHEP** **2203**, 182 (2022), [arxiv:2107.14180](https://arxiv.org/abs/2107.14180).

[81] S. Abreu, D. Chicherin, H. Ita, B. Page, V. Sotnikov, W. Tschernow and S. Zoia, *All Two-Loop Feynman Integrals for Five-Point One-Mass Scattering*, **Phys. Rev. Lett.** **132**, 141601 (2024), [arxiv:2306.15431](https://arxiv.org/abs/2306.15431).

[82] R. Rodrigues, *Two-loop integrals of half-BPS six-point functions on a line*, **JHEP** **2405**, 007 (2024), [arxiv:2402.08463](https://arxiv.org/abs/2402.08463).

[83] J. M. Henn, A. Matijašić, J. Miczajka, T. Peraro, Y. Xu and Y. Zhang, *A computation of two-loop six-point Feynman integrals in dimensional regularization*, **JHEP** **2408**, 027 (2024), [arxiv:2403.19742](https://arxiv.org/abs/2403.19742).

[84] S. Abreu, D. Chicherin, V. Sotnikov and S. Zoia, *Two-loop five-point two-mass planar integrals and double Lagrangian insertions in a Wilson loop*, **JHEP** **2410**, 167 (2024), [arxiv:2408.05201](https://arxiv.org/abs/2408.05201).

[85] S. Abreu, P. F. Monni, B. Page and J. Usovitsch, *Planar six-point Feynman integrals for four-dimensional gauge theories*, **JHEP** **2506**, 112 (2025), [arxiv:2412.19884](https://arxiv.org/abs/2412.19884).

[86] M. Beccetti, C. Dlapa and S. Zoia, *Canonical differential equations for the elliptic two-loop five-point integral family relevant to $t\bar{t}$ +jet production at leading color*, **Phys. Rev. D** **112**, L031501 (2025), [arxiv:2503.03603](https://arxiv.org/abs/2503.03603).

[87] G. Papathanasiou, *The SAGEX review on scattering amplitudes. Chapter 5: Analytic bootstraps for scattering amplitudes and beyond*, **J. Phys. A** **55**, 443006 (2022), [arxiv:2203.13016](https://arxiv.org/abs/2203.13016).

[88] S. He, Z. Li, R. Ma, Z. Wu, Q. Yang and Y. Zhang, *A study of Feynman integrals with uniform transcendental weights and their symbology*, **JHEP** **2210**, 165 (2022), [arxiv:2206.04609](https://arxiv.org/abs/2206.04609).